Accepted Manuscript

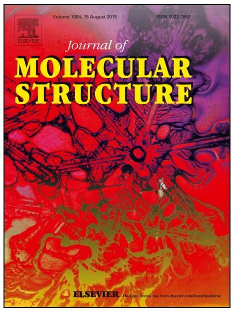

Molecular structure, NMR, UV-Visible, Vibrational spectroscopic and HOMO, LUMO analysis of (E)-1-(2, 6-bis (4-methoxyphenyl)-3, 3-dimethylpiperidine-4-ylidene)-2-(3-(3, 5-dimethyl-1H-pyrazol-1-yl) pyrazin-2-yl) hydrazine by DFT method

A.Therasa Alphonsa, C. Loganathan, S.Athavan Alias Anand, S. Kabilan

PII: S0022-2860(15)30410-5

DOI: 10.1016/j.molstruc.2015.11.005

Reference: MOLSTR 21955

To appear in: *Journal of Molecular Structure*

Received Date: 13 September 2015

Revised Date: 30 October 2015

Accepted Date: 2 November 2015

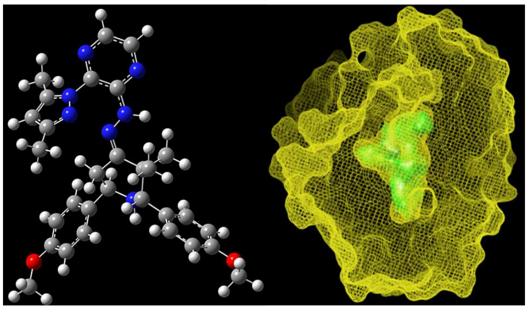

Molecular structure, NMR, UV-Visible, Vibrational spectroscopic and HOMO, LUMO analysis of (E)-1-(2, 6-bis (4-methoxyphenyl)-3, 3-dimethylpiperidine-4-ylidene)-2-(3-(3, 5-dimethyl-1H-pyrazol-1-yl) pyrazin-2-yl) hydrazine by DFT method

A. Therasa Alphonsa[a], C. Loganathan[a], S. Athavan Alias Anand[a], S. Kabilan[a*]

[a]*Department of Chemistry, Annamalai University, Annamalainagar - 608002, Tamilnadu, India.*

Abstract

We have synthesized (E)-1-(2, 6-bis (4-methoxyphenyl)-3, 3-dimethylpiperidine-4-ylidene)-2-(3- (3, 5-dimethyl-1H-pyrazol-1-yl) pyrazin-2-yl) hydrazine (PM6). It was characterized using FT-IR, FT-Raman, ^{1}H NMR, ^{13}C NMR techniques. To interpret the experimental data, *ab initio* computations of the vibrational frequencies were carried out using the Gaussian 09 program followed by the full optimizations done using Density Functional Theory (DFT) at B3LYP/6-311 G(d,p) level. The combined use of experiments and computations allowed a firm assignment of the majority of observed bands for the compound. The calculated stretching frequencies have been found to be in good agreement with the experimental frequencies. The electronic and charge transfer properties have been explained on the basis of highest occupied molecular orbitals (HOMOs), lowest unoccupied molecular orbitals (LUMOs) and density of states (DOS). The absorption spectra have been computed by using time dependent density functional theory (TD-DFT). ^{1}H and ^{13}C NMR spectra were recorded and ^{1}H and ^{13}C NMR chemical shifts of the molecule were calculated using the gauge independent atomic orbital (GIAO) method. From the optimized geometry of the molecule, molecular electrostatic potential (MEP) distribution, frontier molecular orbitals (FMOs) of the title

[*] Corresponding author: Dr. S. Kabilan

Email: profdrskabilanaa@gmail.com, Tel: 9443924629

compound have been calculated in the ground state theoretically. The theoretical results showed good agreement with the experimental values.

Keyword: DFT, VEDA, MEP, NLO, Potential energy scan and Molecular Docking

1. Introduction

Nitrogen and oxygen containing heterocyclic compounds have received considerable attention due to their wide range of pharmacological activity [1]. Pyrazole is an important aromatic heterocyclic compound containing two bonded nitrogen atoms. It is related to many compounds such as isoxazole, isothiazole, oxazole and imidazole [2]. Pyrazoles have illustrious history; in 1883, a German chemist Ludwig Knorr was the first to discover antipyretic action of pyrazole derivative in man, he named the compound antipyrine. When he attempted to synthesize quinoline derivatives with antipyretic activity, accidentally obtained antipyrine (2, 3-dimethyl-1-phenyl-3-pyrazolin-5-one) which has analgesic, antipyretic and antirheumatic activity; which stimulated interest in pyrazole chemistry. The first natural pyrazole derivative was isolated by Japanese workers Kosuge and Okeda in the year 1954, till their discovery it was thought that pyrazoles could not be obtained naturally. They isolated 3-n-nonylpyrazole [3] from Houttuynia Cordata, a plant of the "piperaceae" family from tropical Asia; which showed antimicrobial activity. They also isolated levo-β-(1-pyrazolyl) alanine [4] an amino acid from watermelon seeds (Citrullus Vulgaris).

Many natural products have the pyrazole unit as the core structure [5]. Pyrazoles and its derivatives, a class of well known nitrogen heterocycles, occupy as the core in a variety of leading drugs such as Celebrex, Sildenafil (Viagra), Ionazlac, Rimonabant and Difenamizole etc. Pyrazole analogues have found use as building blocks in organic synthesis for designing pharmaceutical and agrochemicals; and as bifunctional ligands for metal catalysis. Pyrazole and its derivatives have widespread applications in the field of medicine and industry. They are used as antihypertensive [6], anti thrombotic [7], anti inflammatory [8], anti microbial [9], anti rheumatic [10], anti tumor [11], anti viral [12] and anti diabetic [13]. Some derivatives are used as anti corrosion and for coloured photography. These derivatives have attracted significant attention because of the application in drug development [14]. Particularly, arylpyrazoles are important in medicinal and pesticidal chemistry [15]; a number of herbicides with pyrazole moieties have been commercialized [16]. Recent literature shows that, some arylpyrazoles were reported to have non-nucleoside HIV-1 reverse transcriptase inhibitor activity [17, 18]. They are also useful intermediates for many industrial products [19–21]. The vibrational spectra of pyrazole have been thoroughly investigated [22-24], however, there is relatively little information regarding substituted pyrazoles, and N-substituted pyrazoles in particular [25, 26]. The inclusion of a substituent group in pyrazole leads to the variation of charge distribution in molecules and consequently this affects the structural, electronic and vibrational parameters. The methyl and amino groups are generally referred to as electron donating substituents in aromatic ring systems [27]. The CH_3 and NH_2 interact with nearby π systems via hyper conjugation, which implies electronic delocalization and are taken into account by the molecular orbital approach [28, 29].

Due to the importance of the pyrazole nucleus, we believed it worthwhile to design and synthesize new pyrazole derivatives. Investigations into the structural stability of these compounds using both experimental techniques and theoretical methods have been of interest for many years. With recent advances in computer hardware and software, it is possible to correctly describe the physico- chemical properties of molecules from first principles using various computational techniques [30]. In recent years, density functional theory (DFT) has been the shooting star in theoretical modeling.

A large number of studies have been made on the synthesis, spectroscopic analysis and theoretical calculations of pyrazole and its derivatives [31-33]. In this study, we present the experimental and theoretical studies of the title compound. The interaction energies, NMR spectral analysis, Molecular electrostatic potential, thermodynamic and nonlinear optical properties of PM6 were investigated at the B3LYP/6-311G (d, p) level. A detailed interpretation of the vibrational spectra of PM6 has been made on the basis of the calculated amount of total energy distribution (TED) [34]. The results of the theoretical and spectroscopic studies are reported here. The redistribution of electron density (ED) in various bonding and anti-bonding orbitals and E (2) energies has been calculated by natural bond orbital (NBO) analysis. The UV spectroscopic studies along with HOMO, LUMO analysis have been used to elucidate information regarding charge transfer within the molecule. The molecular first hyperpolarizability and thermodynamic properties have been analyzed by means of vibrational spectroscopy. The aim of this work is to explore the molecular dynamics and the structural parameters that govern the chemical behaviour, and to compare predictions made from theory with experimental observations.

2. Experimental

2.1. Synthesis

2, 3-dichloro pyrazine, ammonium acetate, 4-methoxy benzaldehyde, 3-methyl-2-butanone are purchased from Sigma-Aldrich chemical company with a stated purity and are used as such without further purification. The title compound is synthesized according to Scheme 1.

2.2. Instruments

The FT-IR spectrum of the molecule is recorded in the region of 4000-400 cm^{-1} on Thermo Scientific Nicolet iS5 (iDl transmission) using KBr pellet. FT-Raman spectrum is recorded using 1064 nm line of Nd: YAG laser as excitation source with wave length in the region 3500-50 cm^{-1} on a Bruker RFS 100/S FT-Raman spectrophotometer. The detector is a liquefied nitrogen cooled Ge detector. The Ultraviolet absorption spectra of PM6 dissolved in DMSO are examined in the range of 200-800 nm using a Hitachi model U-2001 spectrophotometer. NMR spectrum is performed in Bruker DPX 400 MHz at 300K. The compound is dissolved in DMSO-d6. Chemical shifts are reported in ppm relative to tetramethylsilane (TMS) for protons and carbons. ^{1}H and ^{13}C NMR spectra are obtained at a base frequency of 400 MHz and 100 MHz respectively.

2.3. Computational Techniques

All computational studies are carried out at Density Functional theory (DFT) level on a Dell workstation equipped with V3 quardcore, Xeon quad core processor E3–1240, 3.40 GHz personal computer with 8 GB total RAM using Gaussian 09W program package [35]. DFT calculations are less time consuming and include a significant part of the electron correlation leading to good accuracy. The calculations are carried out with the Becke's three parameter exchange functional with the LYP correction (B3LYP) and the basis set, 6-311 G (d, p) are used in appropriate calculations [36, 37]. The computational work has begun with the conformational analysis of the compound. The selected geometric parameters of the optimized structure of PM6 are given in Table 1S.

2.4. Docking Studies

The molecular docking studies reported in this work were performed on a Dell workstation equipped with Xeon processor E3–1225, V2 quardcore, 3.20 GHz personal computer with 8 GB total RAM and with Schrödinger software suite, LLC, New York, 2014 release. The preliminary step for molecular docking is to prepare the protein and ligand to an optimized and minimized structure. The 3D crystallographic structure of human CYP51 protein (PDB ID: 3LD6) was downloaded from the protein data bank (www.rcsb.com). The complex was prepared by *protein preparation wizard* [38] incorporated in the *Maestro* [39] of Schrödinger software, 2014. After pre–processed, the protein complex was optimized and minimized using *Optimized Potential for Liquid Simulations (OPLS–2005) force field* [40] until the root mean square deviation (RMSD) reached the value of 0.3 Å. Further, the grid was generated for protein complex using receptor grid generation option which is incorporated in the *Glide* [41] module of Maestro. The ligand preparation was done by importing the 2D structure of the compound (mol format) to project table of Maestro. Later, the compound structure was minimized and possible conformers were generated by OPLS–2005 force field using *Ligprep* [42] application. The interactions of the tested ligand in the binding site of the 3LD6 protein were identified by the extra precision (XP) mode of docking using Glide module.

3. Results and Discussion

3.1. Vibrational analysis

The synthesized PM6 is subjected to FT-IR, FT-Raman spectral analysis. The theoretical vibrational analysis of the compound PM6 is analyzed using DFT/B3LYP 6-311 G (d, p) method. The observed and calculated FT-IR, FT-Raman spectrum of PM6 is given in Figure 1S and the values are tabulated in Table 2S. The non-negative vibrational frequency obtained from DFT calculations confirms that the optimized geometry of compound PM6 is located at the minima on the potential energy state. The calculated vibrational frequencies are found to be in good agreement with the observed FT-IR frequencies. The theoretical vibrational frequencies obtained for compound PM6 is interpreted by means of Total energy distribution (TED %) calculations using SQM method. The normal modes assignment of the theoretical frequencies is visualized and substantiated with the help of the GaussView 5.0 visualization program. The synthesized PM6 consists of 74 atoms and hence has 216 normal modes of vibrations which include 78 stretching, 81 bending and 57 torsional modes of vibration. The molecule PM6 belongs to C1 symmetry. All the modes are IR active modes. The significant normal modes with TED (10%) are given in order of decreasing wave numbers in Table 2S.

N-H vibrations

The $\nu_{N\text{-}H}$ stretching vibrations normally appear in the range of 3500-3300 cm^{-1} [43]. The experimental wave number of 3412 cm^{-1} in the FT-IR spectrum (FT-Raman at 3425 cm^{-1}) of PM6 is attributed for N-H stretching. The theoretical N-H stretching vibration modes are visualized in the mode numbers 199 and 198 with the scaled frequencies 3438 cm^{-1} to 3436 cm^{-1} respectively. Both the theoretical and experimental vibrational frequencies are pure vibrations with TED of 99 %.

Aromatic stretching group vibrations

In general, the aromatic C-H stretching frequencies appear in the range of 3100-3000 cm^{-1} [44] and the ring C-C stretching vibrations occur in the region 1650-1400 cm^{-1} [45]. In the present work, the experimental FT-IR spectrum of PM6 the band appeared in the range of 3132 cm^{-1} while in FT-Raman at 3133 cm^{-1} is assigned to the aromatic C-H stretching. In theoretical calculation, the mode nos. 197-186 corresponds to theoretical aromatic C-H stretching vibrations. The theoretical C-C stretching vibration modes are visualized in the mode numbers 163-159 with the scaled frequencies of 1611-1559 cm^{-1} respectively.

Methyl, methylene group vibrations

The symmetric and asymmetric stretching mode of the methyl group appears in the range of 2935-2860 cm^{-1} and 2985-2925 cm^{-1} [46]. The methyl groups present in PM6 undergoes vibrations like symmetric stretching, asymmetric stretching, symmetric and asymmetric bending modes. The C-H stretching vibrations of methyl groups in PM6 are observed in the range at 2983-2924 cm^{-1} in FT-IR spectrum (FT-Raman at 2983, 2944 and 2923 cm^{-1}). The stretching in the methyl groups is well explained by the mode numbers 178-171 in the theoretical vibrational study of the compound PM6. The theoretical wave numbers matched well with the experimental FT-IR and FT-Raman wave numbers. The bending vibrations of the methyl group are found to appear in the region of 1465-1440 cm^{-1} and 1390-1370 cm^{-1} [47]. The bending vibrations of the methyl groups are observed at 1413 cm^{-1} in FT-IR spectrum whereas in FT-Raman spectrum at 1407 cm^{-1} (mode no. 136). The theoretical study make clear of these bending vibrations as asymmetric and symmetric bending vibration of the methyl group with the help of the mode numbers 154-139 and 136 in the scaled frequency range of 1479-1435 and 1414 cm^{-1}.

The asymmetric and symmetric C-H stretching in methylene group normally appears in the region of 3100-2900 cm^{-1} [48]. In the present study, the observations of asymmetric and symmetric stretching of the C-H in methylene group (C16) in compound PM6 observed at 3059 cm^{-1} in FT-IR spectrum (FT-Raman at 3053 cm^{-1}) are complemented by the theoretical investigation which well explains the asymmetric and symmetric stretching in the methylene group in the respective scaled frequencies at 3012 cm^{-1} (mode no.188).

C=N Vibrations

The C=N vibration normally appears in the region 1689-1471 cm^{-1} [49]. The strong band observed at 1612 cm^{-1} in FT-IR spectrum besides in FT-Raman spectrum at 1612 cm^{-1} (mode no. 164) of PM6 is assigned to C=N vibration. The mode no. 164 and 158 with the scaled frequency 1612 and 1541 cm^{-1} visualizes to the C=N stretching.

N-N Vibrations

The wave number of 1120 and 1076 cm^{-1} in the FT-IR spectrum whereas in FT-Raman spectrum at 1123 and 1079 cm^{-1} (mode nos.101 and 97) is attributed for N-N stretching in pyrazine ring and in NH-N bond. The N-N stretching vibration modes are visualized in the mode nos. 96, 97 and 100-102 with the scaled frequency 1064, 1089, 1107, 1124 and 1129 cm^{-1} respectively.

3.2. ^{1}H and ^{13}C NMR spectral analysis.

The ^{1}H NMR spectrum of PM6 has been given in Figure 2S. In the ^{1}H NMR spectrum of the compound PM6 Table 1 in which H (4) signal appears as triplet at 0.85 ppm. The singlet at 1.20 ppm in the ^{1}H NMR indicates the presence of H (3). The doublet at 2.54 ppm in the ^{1}H NMR spectrum of the compound PM6 shows the presence of H (16) protons. The ^{1}H NMR spectrum of PM6 reveals a multiplet at 4.78 ppm for H (5), H (15) attached to a phenyl ring. The aromatic protons are observed in the range for 6.92 to 7.59 ppm. The doublet observed at 9.92 and 10.03 ppm are attributed to the presence of H (26) and H (14) ppm.

The ^{13}C NMR spectrum of the compound PM6 has been displayed in Figure 3S. The carbon chemical shifts are presented in Table 1. The ^{13}C NMR spectrum of the synthesized compound PM6 has been recorded in DMSO. The low field signal observed at 20.1 and 20.9 ppm in ^{13}C NMR spectra of PM6 is due to the carbons C 38, C39. The C (16) carbon is identified at 47.7 ppm in ^{13}C NMR of PM6. The carbons in the azine linkage are exposed by the up-field signals 159.6 ppm to 160.1 ppm. The signals at 58.1 ppm and55.2 ppm in the ^{13}C NMR spectrum of PM6 are due to the carbons C (15) and C (2) respectively.

NMR spectroscopy is the key to reveal the conformational analysis of organic molecules. Good quality geometries must be taken into consideration for the quantum calculation of the absolute isotropic magnetic shielding tensors to yield more reliable results. There are many reports on NMR isotropic magnetic shielding tensor calculations employing the GIAO method associated with the Density functional theory (DFT) [50]. The GIAO ^{1}H NMR and ^{13}C NMR chemical shift calculations of the stable conformer is made in DMSO [scrf= (solvent=DMSO)] using B3LYP / 6-311G (d, p) basis set. The isotropic values in the calculations are subtracted from a scaling factor of 182.4656 and 31.882 to obtain the chemical shifts for ^{13}C and ^{1}H NMR respectively. The obtained chemical shift values were compared with the experimentally observed values. The observed and the calculated chemical shift values are found to be in good agreement. The calculated values are given in the Table 1 along with the observed values. The relationship between the experimental chemical shift and computed chemical shift values are given in Figure 2. The relation between the observed and computed values predicts that the conformation deducted theoretically should be the favorable conformation of the synthesized PM6.

3.3. Natural Bond orbital analysis

The natural bond orbital analysis provides an efficient method for studying intra-and intermolecular bonding and interaction among bonds, and also provides a convenient basis for investigating charge transfer or conjugative interaction in molecular systems; it could enhance the analysis of the delocalization of charge in the system.

The donor bonding orbitals, the acceptor antibonding orbitals, the donor lone pair atoms are given in Table 2 along with the E (2) values which estimates the interaction between the donor (filled) and acceptor (vacant) orbitals. The E (2) energy is the lowering energy that occurs during the hyperconjugative electron transfer process and hence E (2) can be referred to as stabilization energy. Larger the E (2) values, greater is the stability of the molecule. In the NBO analysis of the compound PM6, the E (2) values are greater for the delocalization of the electrons between the bonds present in the phenyl ring. The lone pair of electrons present in the Nitrogen atom N25, N26, N33, N32, N29, O12, O23 are delocalized to C1-C16, C1-N25, C27-N32, C28-N29, C37- C36, C35- N34, C27- C28, C27-C28, C10- C9 and C21-C20 antibonding orbitals. The delocalization energy for lone pair electrons delocalization to π^* antibonding orbital is higher than the delocalization of lone pair electrons to σ^* antibonding orbitals.

3.4. Charge Analysis

The charge quantifies the electronic structure changes under atomic displacement. It is related directly to the chemical bonds present in the molecule, it influences dipole moment, polarizability, electronic structure and more properties of molecular systems. The Mulliken and natural charge distribution of the molecule calculated on B3LYP level with 6-311G (d, p) basis set are shown in Table 3. The Mulliken charge distribution in the compound PM6 is found to be the distribution of charges considering the atomic orbitals alone and the natural charge distribution considers the polarization of the orbitals too and hence some atoms like C2, C3, C4, C13, N14C16, C21C24, C35, C37, C38 and C39 possess great differences between Mulliken and natural charges Figure 3. The carbon atoms 5C, 6C, 15C, 17C, 30C, 31C possess positive Mulliken charge and negative natural charge. All the hetero atoms in the compounds possess negative Mulliken and negative charges.

3.5. Molecular electrostatic potential (MEP) surfaces

The reactive behavior of the molecule is visualized with the help of three dimensional MEP surface. MEP surface describes the charge distribution in the molecule and helps in predicting the sites for nucleophilic and electrophilic attack in the molecule. The MEP surface has been plotted for the molecules PM6 in Figure 4. Region of negative charge is pictured out in red colour and it is found around the electronegative N in the azine linkage and O12, O23 atoms in the methoxy groups in the molecule PM6. The red colour region is susceptible to electrophilic attack. The blue colour region represents strong positive region and is prone to nucleophilic attack. The green colour region corresponds to a potential half way between the two extremes red and blue region.

3.6. HOMO-LUMO of PM6

HOMO-LUMO pictures of molecule PM6 is presented in Figure 5. The p_z orbitals of O23, O12, C13, C24, C22, C17, C18, C19, C20, C21, N14, C5, C6, C7, C8, C9, C10, C11, C15 carbon atoms do not involve in the formation of the HOMO orbitals in the molecule PM6. The p_z orbitals of O23, O12, C13, C24 ,C22, C17, C18, C19, C20, C21, C7, C8, C9, C10, C11, C4 carbon atoms alone do not involve in the formation of the LUMO orbital. The band gap between the HOMO and LUMO orbital energy is found to be 4.140 eV.

3.7. Polarizability calculations of PM6

The calculated values of the dipole moment (μ), the polarizability (α_0) and first hyperpolarizability (β_{tot}) by finite field approach are given in Table 4 along with the corresponding components. The field independent and field dependent dipole moment μ values of PM6 are calculated to be 4.84 and 1.64 respectively. The highest value of dipole moment is observed for the component μ_X for both the field independent and dependent conditions. The compound PM6 is found to be polar molecule having non – zero dipole moment components.

The calculated polarizabilities α_{ij} have non – zero values and are dominated by the diagonal components. The β_{tot} value of PM6 is found to be 10.81 x 10^{-30} esu. Delocalization of charges in particular directions is indicated by large values of those particular components of polarizability and hyperpolarizability. First order hyperpolarizability is dominated by β_{xxx} value. This shows that the delocalization of the charges in presence of external field is endorsed in β_{xxx} direction. The first hyperpolarizability of PM6 (β_{tot}) is 29 times greater than that of urea (0.3728 x 10^{-30} esu); hence this molecule can have considerable NLO activity.

3.8. UV spectrum and electronic properties

On the basis of fully optimized ground-state structure, TD-DFT// B3LYP/6-311 G (d, p) calculations have been used to determine the low-lying excited states of PM6. The experimental λ_{max} value is obtained from the UV/Vis spectra recorded in DMSO is given in Figure 4S. The calculations were also performed with DMSO solvent effect. The calculated results involving the vertical excitation energies and wavelength are carried out and compared with measured experimental wavelength. Typically, according to the Franck-Condon principle, the maximum absorption peak (max) corresponds in an UV-Vis spectrum to vertical excitation. The TD-DFT// B3LYP/ 6-311 G (d, p) [51] method predicts one intense electronic transition at 280 nm in good agreement with the measured experimental data (exp=283nm). The deviation between experimental and theoretical results may be due to solvent effects. This electronic absorption corresponds to the transition from the ground to the first excited state and is mainly described by one electron excitation from the highest occupied molecular orbital (HOMO) to the lowest unoccupied molecular orbital (LUMO). The HOMO-LUMO energy gap of PM6 was calculated at the B3LYP/6-311 G (d, p) level. LUMO as an electron acceptor represents the ability to obtain an electron; HOMO represents the ability to donate an electron. The gap between HOMO and LUMO characterizes the molecular chemical stability [52]. The energy gap between the HOMOs and LUMOs is a critical parameter in determining molecular electrical transport properties because it is a measure of electron conductivity.

3.9. Docking studies

Molecular docking studies were performed to investigate the binding affinities of the newly synthesized compound PM6 and the human CYP51 protein, PDB ID: 3LD6 [53]. The ligand−protein complex stability was successfully made by some features such as hydrogen bond interactions, vander Waals forces, $\pi-\pi$ stacking, hydrophilic and hydrophobic interactions. These interactions between the drug and receptor depend upon the nature of functional groups present in the ligand. On ligand preparation (by *ligprep* module) of compound PM6, twelve structures were obtained as different conformers. Each conformer was docked into the binding pocket of the 3LD6. The conformer with high docking score -8.41 is displayed in Fig. 6. The imidazole and pyrazine nucleus of the tested compound PM6 have two π−π stacking interactions with TYR 131 and PHE 234 amino acids respectively. The docking studies were also showed weak hydrogen bond interaction with length 2.27 Å between the pyrazine nitrogen atom of PM6 and the water molecule (HOH 8) present in the active site of 3LD6. The statistical parameters of top five conformers of compound PM6 were tabulated in Table 5.

4. Conclusions

A novel compound PM6 was synthesized and characterized by FT-IR, UV, FT-Raman, ^{1}H and ^{13}C NMR techniques. The theoretical vibrational frequencies are found to be in good agreement with the observed vibrational frequencies of PM6. The compound PM6 is subjected to NBO analysis, the E(2) values are greater for the delocalization of the electrons between the bonds present in the phenyl ring. The delocalization energy for lone pair electrons delocalization to π* antibonding orbital is higher than the delocalization of lone pair electrons to σ* antibonding orbitals. The first hyper polarizability of PM6 is 29 times greater than of urea (0.3728 x 10^{-30} esu), hence this molecule can have considerable NLO activity and can find its application in material science field too. The docking results clearly indicate that the imidazole and pyrazine nucleus of the tested compound PM6 have two π−π stacking interactions with TYR 131 and PHE 234 amino acids present in the active site of 3LD6.

References

[1] P.M.G. Swamy, Y.S. Agasimundin, Rasayan J. Chem. 1 (2) (2008) 421–428.

[2] B.K.Wibreg "Aromaticity of Heterocyclic Chemistry; pyrazole, pyrazolines, pyrazolidines imidazoles and condensed ring" 3, 20 (1967); B.K.Wibreg "Aromaticity and its chemical Manifestation" (1999) 519.

[3] Da-Qing Shi, Jing-Wen Shi, Hao Yao, J Chinese Chem. Soc *56* (2009) 504-509.

[4] Hai-Ling Liu, Huan-Feng Jiang, Min Zhang, Wen-Juan Yao, Qiu-Hua Zhu, Zhou Tang, Tetrahedron Lett 49 (2008) 3805-3809.

[5] J. Elguero, A.R. Katrinsky, C.W. Rees, E.F.V. Scriven (Eds.), Comprehensive Heterocyclic Chemistry, vol. 7, Pergamon, Oxford (1996) 1.

[6] T.Irikura, M.Hayashi, K.Kotare, Y.Kudus, J.Hatayama and E. Hetaugi, Jap.Patent.Chem. 714 (1997) 799.

[7] R.L. Bick, J. Fareed and D. Hoppensteadt "New antithrombotic drugs: A perspective.Curr opin cardiovasc pulmonary Renal Invest Drugs” 1 (1999) 40-55.

[8] K.S. Sahu, M. Bouerjee, A. Samantray, C. Behera and A.M. Azam, Tropical J.Pharma Res; 7 (2008) 961-968.

[9] S.B. Holla, M. Mahalinga, S.M. Karthikeyan, M.P. Akberali and S.N. Shetty, Bioorg. Med. Chem. 14 (2006) 2040-2047.

[10] A.R. Katritzky, A.V.Vakulenko, R.A.Gedu and J.W.Rogers, ARKIVOC i, 2 (2007) 8555-60.

[11] Li.J. Zhao, Y.F.Zhao, X.L-Yuan and P.Gong, Arch.Pharm.Chem.Live Sci, 339 (2006) 593-597.

[12] Z.R. Yan, Y.X. Liu, F.W.Xu, C. Pannecouque, M. Witvrouw and E. De Clereq, Arch. Pharm. Res. 29 (2006) 957.

[13] A. Perez-Rebolledo, J.D. Ayala, G.M. de Lima,N.Marehini,G. Bo-Mbieri, C.L. Zani, E.M. Souza-Fagundes and H. Beraldo, Eur.J.Med.Chem. 40 (2005) 467.

[14] M.P. Donohue, D.A. Marchuk, H.A. Rockman, J. Am. Coll. Cardiol. 48 (2006) 1289-1298.

[15] W.L. John, R.M. Patera, M.J. Plummer, B.P. Halling, D.A. Yuhas, Pest. Sci. 42 (1994) 29-36.

[16] K. Hirai, A. Uchida, R. Ohno, in: P. Boger, K. Hirai, K. Wakabyashi, K. Herbicide (Eds.), Classes in Development, Springer-Verlag, Heidelberg (2002) 279– 289.

[17] M.J. Genin, C. Biles, B.J. Keiser, S.M. Poppe, S.M. Swaney, W.G. Tarpley, Y. Yagi, D.L. Romero, J. Med. Chem. 43 (2000) 1034-1040.

[18] D. Rambabu, G.R. Krishna, S. Basavoju, C.M. Reddy, M. Pal, J. Mol. Struct. 994 (2011) 332–334.

[19] M.G. Mamolo, D. Zampieri, V. Falagiani, L. Vio, E. Banfi, Il Farmaco 56 (2001) 593–599.

[20] C. Cativiela, J.L. Serrano, M.M. Zurbano, J. Org. Chem. 60 (1995) 3074–3083.

[21] D. Wang, C.Y. Zheng, L. Fan, J. Mol. Struct. 938 (2009) 311–315.

[22] V. Tabacik, V. Pellegrin, H.H. Gunthard, Spectrochimica Acta Part A 35 (1979) 1055-1081.

[23] M. Majoube, J. Raman Spectrosc. 20 (1989) 49-60.

[24] J.R. Durig, M.M. Bergana, W.M. Zunic, J. Raman Spectrosc. 23 (1992) 357-363.

[25] J.M. Orza, O. Mó, M. Yáñez, J. Elguero, Spectrochimica. Acta Part A 53 (1997) 1383-1398.

[26] G. Zerbi, C. Alberti, Spectrochimica. Acta 18 (1962) 407,

[27] B. Ballesteros, L. Santos, Spectrochimica. Acta A 58 (2002) 1069-1081.

[28] W.B. Tzeng, K. Narayanan, J.L. Lin, C.C. Tung, Spectrochimica. Acta 55A (1999) 153-162.

[29] W.B. Tzeng, K. Narayanan, K.C. Shieh, C.C. Tung, J. Mol. Struct. (Theochem) 428 (1998) 231-240.

[30] Y. Zhang, Z.J. Guo, X.Z. You, J. Am. Chem. Soc. 123 (2001) 9378–9387.

[31] M.S. Surendra Babu, K.Rajasekar, K.N.Jayaveera, Indian **J**ournal of **A**dvances in **C**hemical **S**cience **1** (2012) 52-56.

[32] Ifzan arshad1, Muhammad Naeem Ahmed, Journal of Single Molecule Research. 2 (2014) 1-5.

[33] U.H. Patel, S.A. Gandhi, B.D. Patel et al., Indian Journal of Pure and Applied Physics, 51 (2013) 819-826.

[34] A. Nataraj, V. Balachandran, T. Karthick, M. Karabacak and A. Atac, J. Mol. Struct. 1027 (2012) 1-14.

[35] R. Arulmani, R. Balachandar, P. Vijaya, K.R. Sankaran, Spectrochimica Acta Part A: Molecular and Biomolecular Spectroscopy, 138 (2015) 660-666.

[36] C. Lee, W. Yang, R.G. Parr, Phys. Rev. B 37 (1988) 785–789.

[37] A.D. Becke, J. Chem. Phys. 98 (1993) 5648–5652.

[38] Protein Preparation Wizard; *Epik* version 2.3, 2014; *Impact* version 5.7, 2014, Schrödinger, LLC, New York.

[39] Maestro, version 9.3.5, Schrödinger, LLC, New York, 2014.

[40] W. L. Jorgensen, D. S. Maxwell and J. Tirado–Rives, *J. Am. Chem. Soc.*, 1996, **118**, 11225–11236.

[41] Glide version 5.8, 2014, Schrödinger, LLC, and New York.

[42] LigPrep, version 2.5, 2014, Schrödinger, LLC, New York

[43] G. Rauhut, P. Pulay, J. Phys. Chem. 99 (1995) 3093.

[44] A. P. Scott, L. Radom, J. Phys. Chem. 100 (1996) 16502.

[45] Y. Li, Y. Liu, H. Wang, X. Xiong, P. Wei, F. Li, Molecules 18 (2013) 877-893.

[46] H.T. Flakus, A. Miros, P. G.Jones, Spectrochimica Acta Part A 86 (2012) 242-251.

[47] W.B. Tzeng, K. Narayanan, J.L.Lin, C.C.Tung, Spectrochimica Acta Part A 55 (1999) 53- 162.

[48] H.K. Jeong, H.J. Noh, J.Y. Kim, M.H. Jin, C.Y. Park and Y.H. Lee, Euro physics letters 82 (2008) 67004.

[49] S. Higuchi, E, Kuno, S.Tanaka and H. Kamada, Spectrochimica Acta Part A 28 (1972) 1335-1346.

[50] R. Lu, W. Gan, B. Wu, Z. Zhang, Y. Guo and H. Wang, J.phys.chem.B 109 (2005) 14118- 14129.

[51] P. Vijaya and K.R. Sankaran, Spectrochimica Acta Part A 138 (2015) 460-473.

[52] N. Sundaraganesan, C. Meganathan, H.Saleem, B.D. Joshua, Spectrochimica Acta Part A 68 (2010) 259-269.

[53] N. Strushkevich, S. A. Usanov and H. W. Park, *J. Mol .Biol.*, 397 (2010) 1067–1078.

Figure and Scheme Captions

Scheme 1.

Fig. 1. Numbering of PM6 used in this study

Fig. 2. Comparison of observed and theoretical chemical shifts values of ^{1}H and ^{13}C spectrum of PM6

Fig. 3. Comparison of Mulliken charges and NBO charges of PM6

Fig. 4. MEP plot of PM6

Fig. 5. HOMO-LUMO pictures of PM6

Fig. 6. 2D and 3D docking poses of compound PM6 with 3LD6

(i) Synthesis of hydrazine

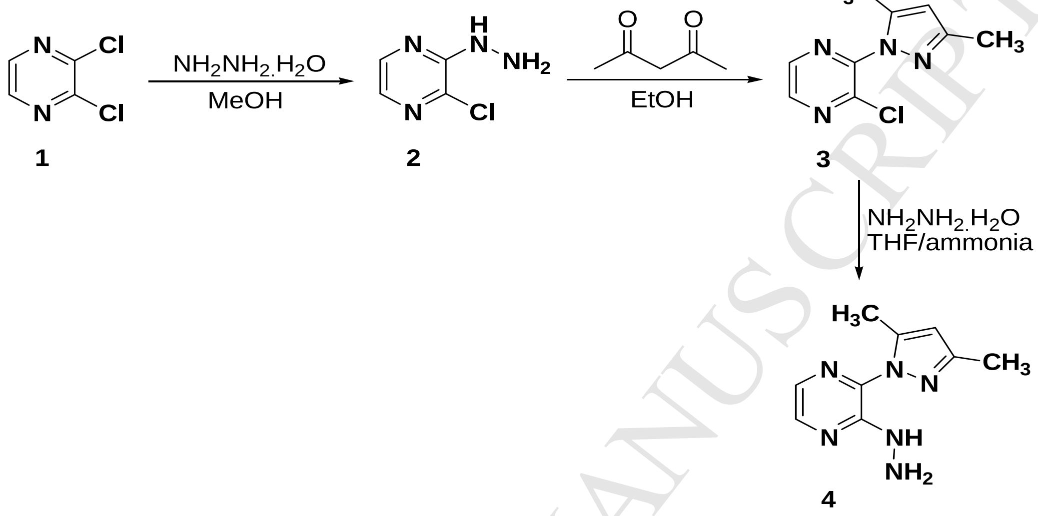

(ii) Synthetic route of PM6

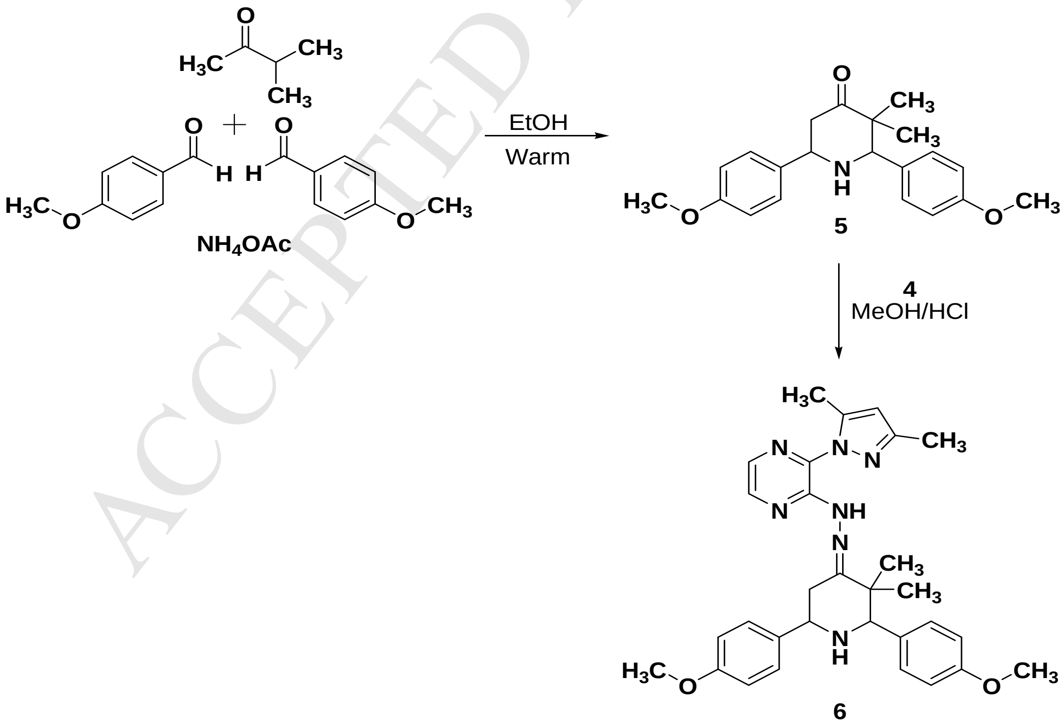

Scheme 1

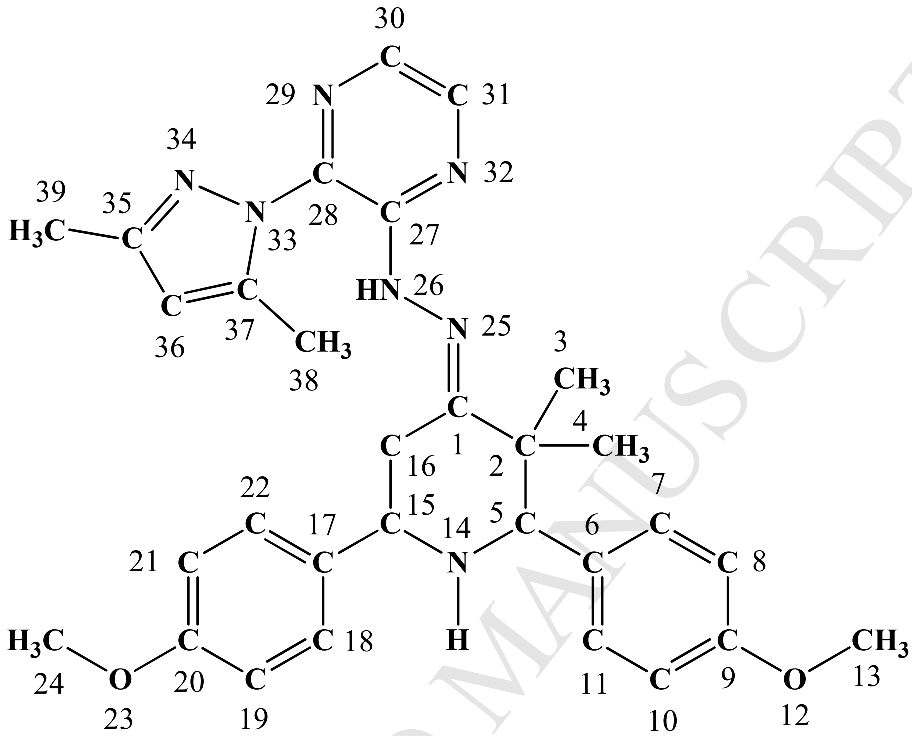

Fig. 1. Numbering of PM6 used in this study

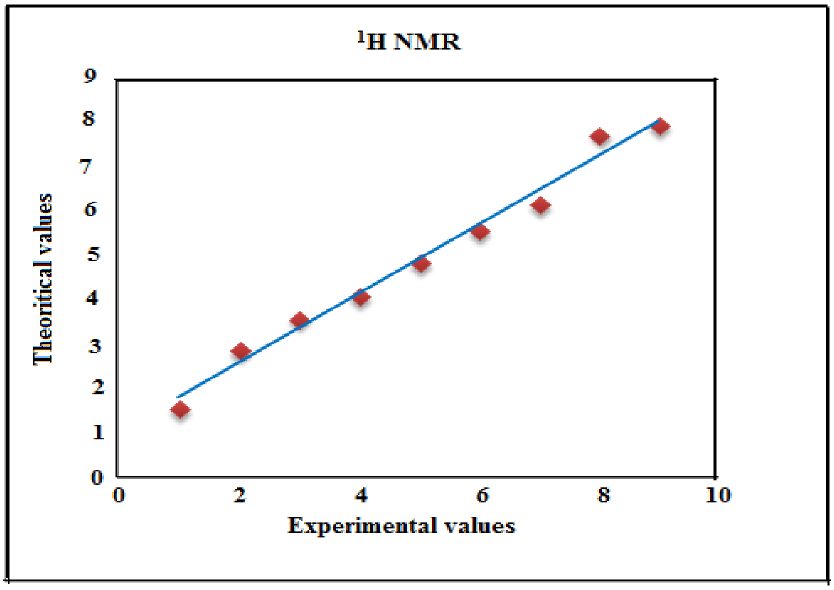

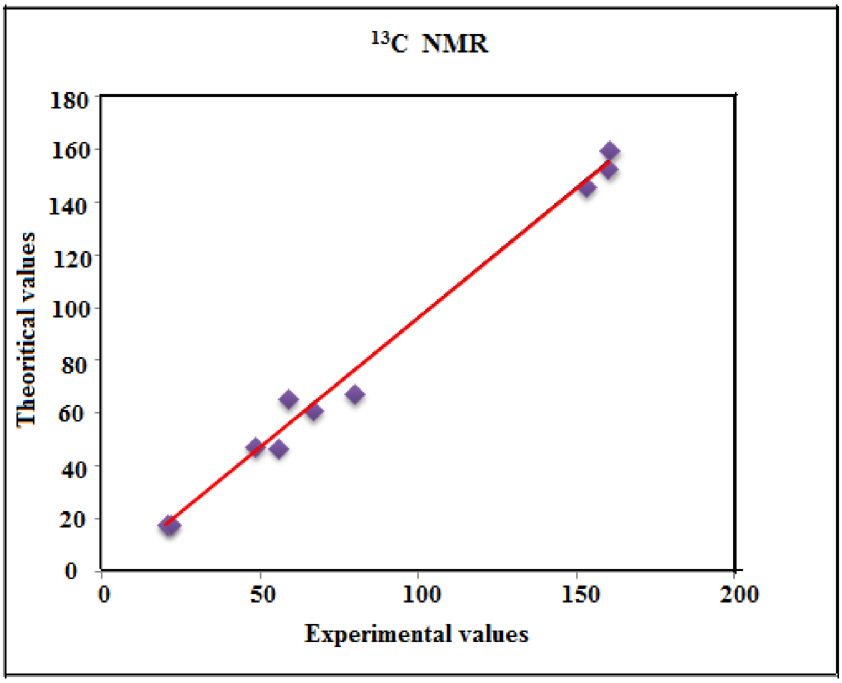

Fig. 2. Comparison of observed and theoretical chemical shifts values of ^{1}H and ^{13}C spectrum of PM6

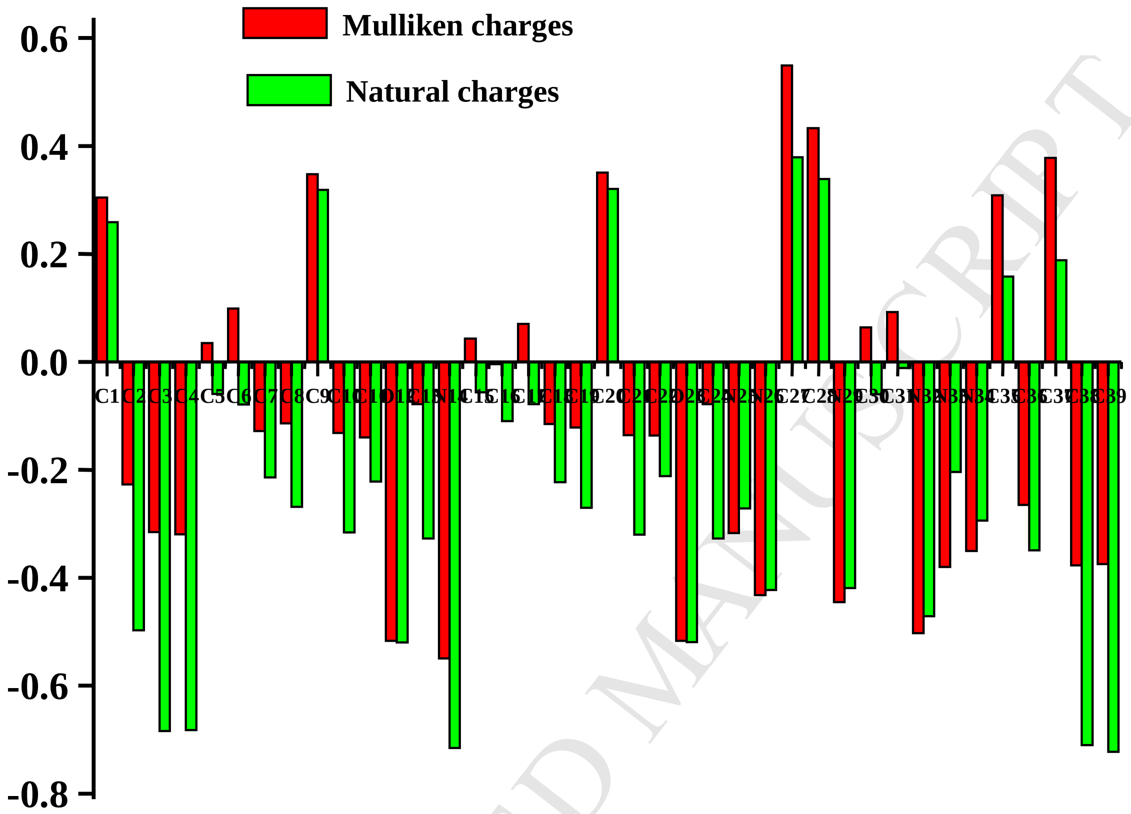

Fig. 3. Comparison of Mulliken charges and Natural charges of PM6

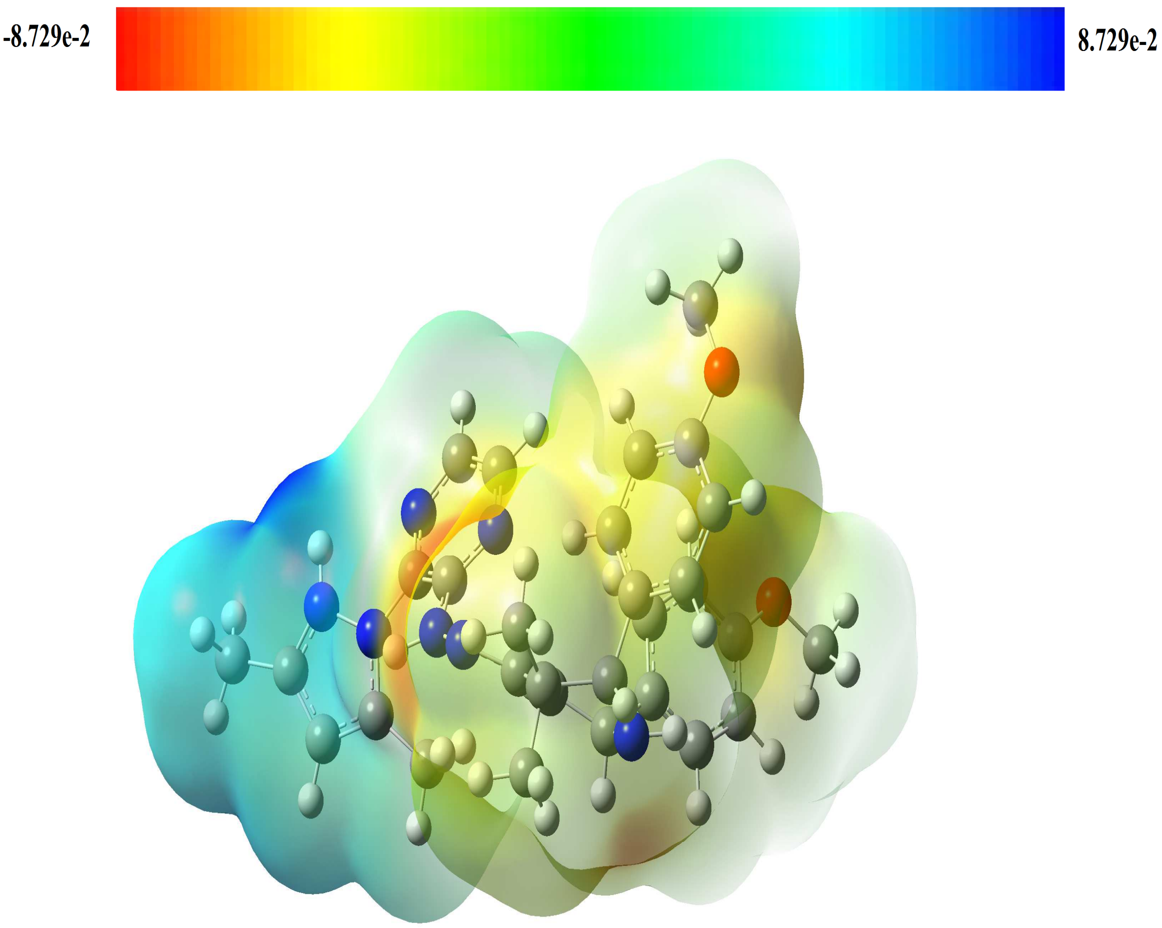

Fig. 4. MEP plot of PM6

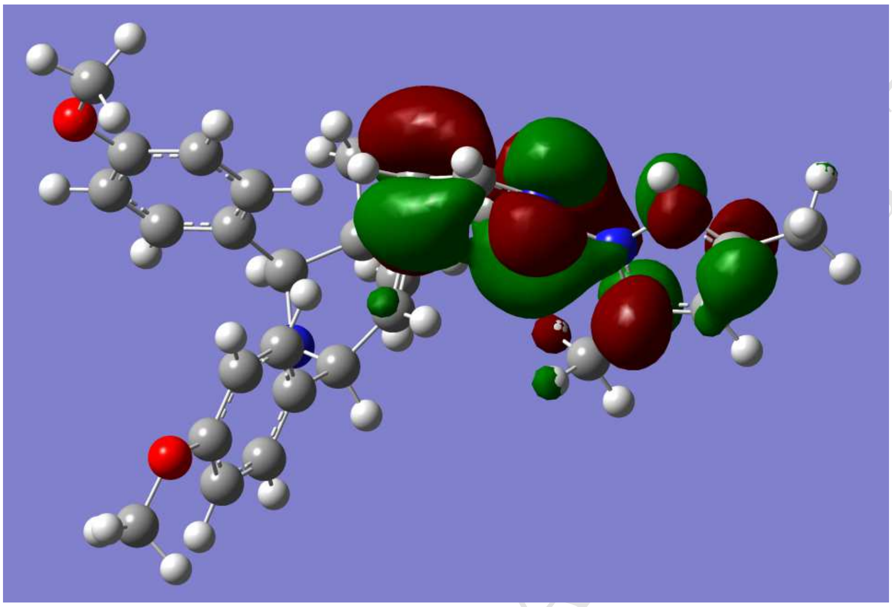

a) **HOMO**

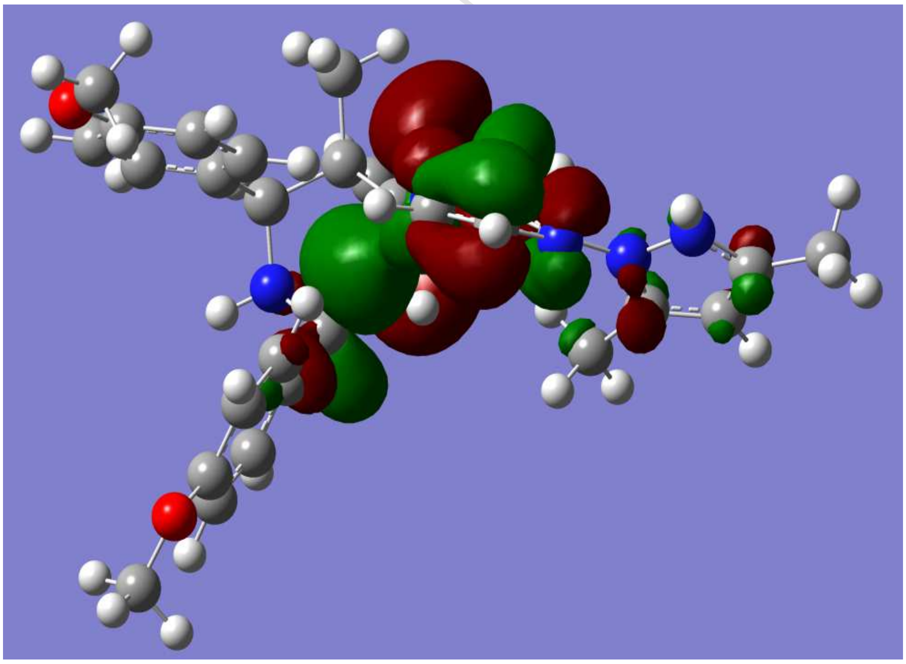

b) **LUMO**

Fig. 5. a) HOMO and b) LUMO pictures of PM6

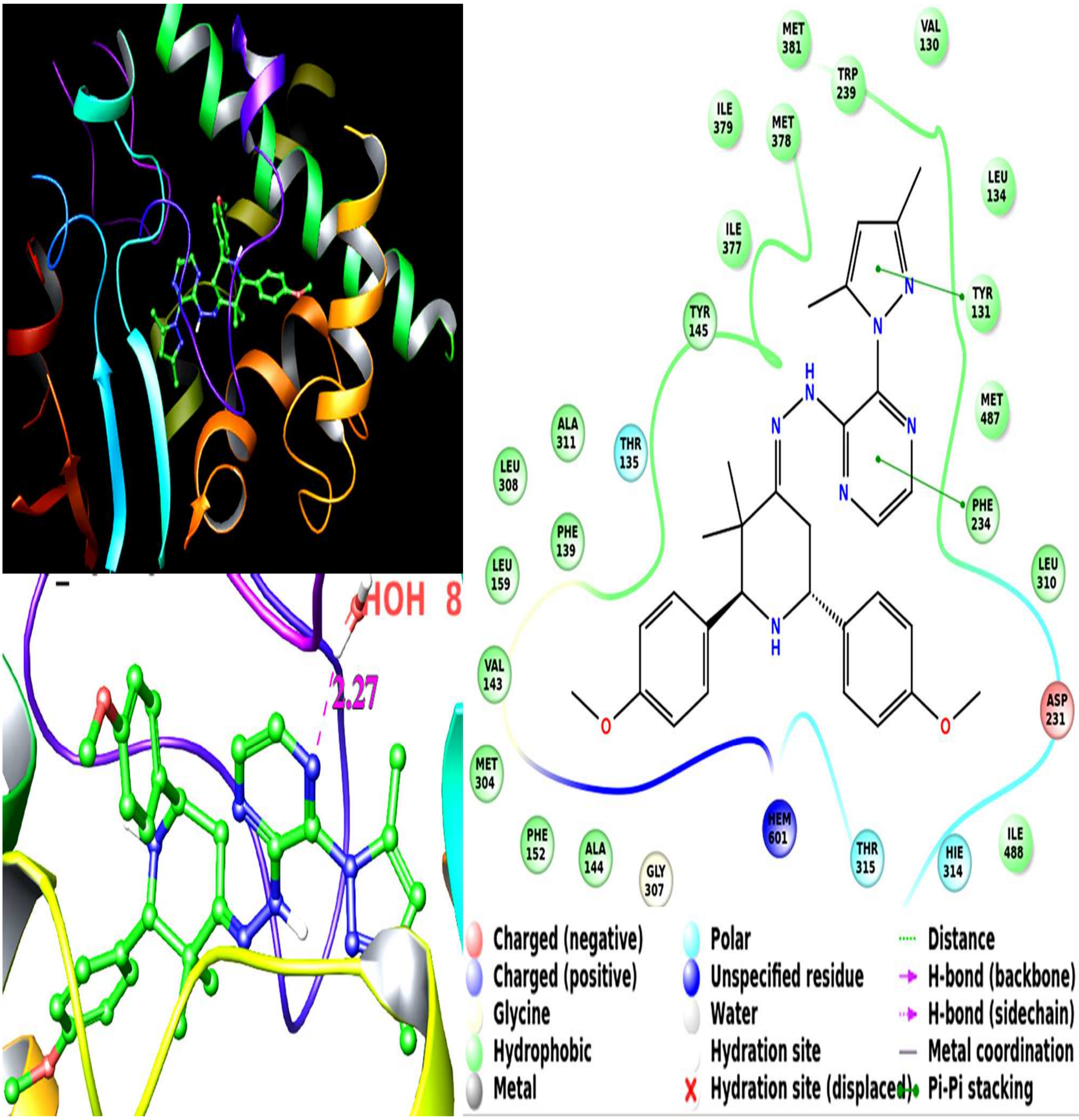

Fig. 6 2D and 3D docking poses of compound PM6 with 3LD6

Table captions

Table 1. Experimental and computational ^{1}H and ^{13}C NMR spectral analysis of PM6 in DMSO solution by DFT method

Table 2. Second order perturbation theory analysis of fock matrix in NBO basis for PM6

Table 3. Mulliken charges and NBO charges of PM6

Table 4. Dipole moment μ (D), mean polarizability α_0 (x 10^{-24} esu) and first hyperpolarizability β_{tot} (x10^{-33} esu) of PM6 by DFT method

Table 5. Molecular docking data of PM6 conformers with 3LD6

Table 1. Experimental and computational ^{1}H and ^{13}C NMR spectral analysis of PM6 in DMSO solution by DFT method.

^{1}H chemical shift values

Atom	Expt. value	Calc. value
H4	0.846(s)	1.569
H3	1.199(s)	2.886
H(38,39)	2.436(s)	2.258
H5	4.782(m)	4.127
H15	4.782(m)	4.871
H(13,24)	3.706(s)	3.755
H(16-Ha,Hb)	2.544(d)	2.227
Aromatic Protons	6.921-7.591	6.833-7.775
H26	9.928(d)	7.992
H14	10.033(d)	0.948

^{13}C chemical shift values

Atom	Expt. value	Calc. value
C39	20.09	12.307
C38	20.93	14.233
C16	47.70	47.822
C2	55.22	47.507
C15	58.09	69.467
C5	66.23	61.768
C13,24	79.16	54.73
Aromatic Carbon	113.48-152.35	109.45-146.38
C27	159.56	153.36
C1	160.13	160.31

Table 2. Second order perturbation theory analysis of fock matrix in NBO basis for PM6.

Type	Donor (i)	ED (i,e)	Acceptor (j)	ED (j,e)	E2 (Kcal/Mol)	E(j)-E(i) a.u	F(i,j) a.u
π - π *	C6-C11	1.67512	C7-C8	0.32255	21.20	0.28	0.069
π - π *	C6-C11	1.67512	C10-C9	0.39583	18.12	0.27	0.064
π - π *	C7-C8	1.70354	C6-C11	0.35770	18.18	0.29	0.065
π - π *	C7-C8	1.70354	C10-C9	0.39583	21.57	0.28	0.071
π - π *	C10-C9	1.65894	C6-C11	0.35770	21.51	0.29	0.071
π - π *	C10-C9	1.65894	C7-C8	0.32255	16.94	0.29	0.063
π - π *	C17-C22	1.68035	C18-C19	0.31555	21.10	0.28	0.069
π - π *	C17-C22	1.68035	C21-C20	0.39327	17.63	0.27	0.063
π - π *	C18-C19	1.70479	C17-C22	0.35414	17.42	0.29	0.064
π - π *	C18-C19	1.70479	C21-C20	0.39327	21.73	0.28	0.071
π - π *	C21-C20	1.66195	C17-C22	0.35414	21.94	0.29	0.072
π - π *	C21-C20	1.66195	C18-C19	0.31555	16.64	0.30	0.063
π - π *	C27-N32	1.69574	C28-N29	0.39068	14.82	0.31	0.062
π - π *	C27-N32	1.69574	C31-C30	0.31050	26.10	0.33	0.083
π - π *	C28-N29	1.75242	C27-N32	0.43411	17.13	0.31	0.068
π - π *	C28-N29	1.75242	C31-C30	0.31050	19.20	0.33	0.073
π - π *	C31-C30	1.63878	C27-N32	0.43411	16.51	0.26	0.060
π - π *	C31-C30	1.63878	C28-N29	0.39068	21.94	0.27	0.069
π - π *	C37-C36	1.79822	C35-N34	0.37900	28.58	028	0.083
π - π *	C35-N34	1.88675	C37-C36	0.32959	11.68	0.33	0.059
LP(2)- π*	O12	1.84157	C10-C9	0.39583	30.60	0.34	0.097
LP(2)- π*	O23	1.84061	C21-C20	0.39327	30.83	0.34	0.097
LP(1)- σ*	N25	1.92136	C1-C16	0.05285	13.58	0.75	0.091
LP(1)- π*	N26	1.69355	C1-N25	0.17099	25.75	0.31	0.082
LP(1)- π *	N26	1.69355	C27-N32	0.43411	42.04	0.27	0.098
LP(1)- π *	N33	1.56148	C28-N29	0.39068	14.67	0.24	0.054

LP(1)- π *	N33	1.56148	C37-C36	0.32959	39.96	0.29	0.099
LP(1)- π *	N33	1.56148	C35-N34	0.37900	25.81	0.28	0.077
LP(1)- σ*	N32	1.91050	C27-C28	0.05404	10.80	0.86	0.087
LP(1)- σ*	N29	1.91011	C27-C28	0.05404	11.39	0.85	0.089
π *- π *	C10-C9	0.39583	C6-C11	0.35770	263.60	0.01	0.079
π *- π *	C10-C9	0.39583	C7-C8	0.32255	277.14	0.01	0.082
π *- π *	C21-C20	0.39327	C17-C22	0.35414	275.58	0.01	0.080
π *- π *	C21-C20	0.39327	C18-C19	0.31555	255.27	0.01	0.082
π *- π *	C27-N32	0.43411	C31-C30	0.31050	119.98	0.02	0.078
π *- π *	C28-N29	0.39068	C31-C30	0.31050	138.24	0.02	0.079
π *- π *	C35-N34	0.37900	C37-C36	0.32959	154.34	0.01	0.067

a - energy of hyper conjugative interaction (stabilization energy), b - energy difference donor and acceptor i and j NBO orbitals, c - F (i-j) is the fock matrix element between i and j NBO orbitals

Table 3. Mulliken charges and Natural charges of PM6

Atom	Mulliken Charges	Natural Charges
1C	0.304	0.258
2C	-0.227	-0.497
3C	-0.315	-0.684
4C	-0.319	-0.682
5C	0.035	-0.059
6C	0.099	-0.079
7C	-0.128	-0.214
8C	-0.114	-0.269
9C	0.348	0.318
10C	-0.132	-0.316
11C	-0.140	-0.222
12O	-0.517	-0.520
13C	-0.078	-0.327
14N	-0.549	-0.715
15C	0.043	-0.056
16C	-0.004	-0.110
17C	0.070	-0.078
18C	-0.115	-0.223
19C	-0.122	-0.270
20C	0.351	0.320
21C	-0.136	-0.320
22C	-0.137	-0.212
23O	-0.517	-0.519
24C	-0.078	-0.327
25N	-0.317	-0.272
26N	-0.432	-0.423
27C	0.549	0.379

28C	0.433	0.339
29N	-0.445	-0.419
30C	0.064	-0.060
31C	0.092	-0.011
32N	-0.503	-0.471
33N	-0.380	-0.204
34N	-0.350	-0.294
35C	0.308	0.158
36C	-0.265	-0.349
37C	0.378	0.188
38C	-0.377	-0.710
39C	-0.375	-0.722

Table 4. The dipole moment μ (D), the mean polarizability <α> (x 10^{-24} esu) and the first hyperpolarizability β_{tot} (x10^{-33} esu) of PM6 by DFT method

Parameters		**Dipole moment**	**Parameters**	**First hyperpolarizability**
μ_x	field independent	-4.15	β_{xxx}	7584.3
	field dependent	-1.57	β_{xxy}	-972.27
μ_y	field independent	1.69	β_{xyy}	1858.297
	field dependent	0.23	β_{yyy}	-1354.88
μ_z	field independent	1.82	β_{xxz}	-1426.34
	field dependent	0.39	β_{xyz}	760.31
μ	field independent	4.84	β_{yyz}	-2235.43
	field dependent	1.64	β_{xzz}	17.42
Parameters		**Polarizability**	β_{yzz}	-1223.87
α_{xx}		66.76	β_{zzz}	-168.80
α_{xy}		-0.88	β_{tot}	10806.24
α_{yy}		61.89		
α_{xz}		-8.33		
α_{yz}		3.46		
α_{zz}		44.13		
<α>		57.60		

α: 1a.u = 0.1482*10^{-24} esu; β: 1a.u = 8.6393*10^{-33} esu

Table 5. Molecular docking data of **PM6** conformers with 3LD6

Conformer	Docking score	Glide score	Glide evdw	Glide ecoul	Glide energy
Conf. 1	-8.41	-9.76	-56.61	-1.69	-58.29
Conf. 2	-7.09	-7.19	-37.83	-3.81	-41.64
Conf. 3	-6.15	-6.25	-51.10	-2.07	-53.17
Conf. 4	-5.33	-6.67	-61.00	-2.53	-63.54
Conf. 5	-5.23	-7.04	-56.64	-0.39	-57.03

SUPPLIMENTARY FIGURES AND TABLES

Figure 1S. Experimental IR spectrum of PM6.

Experimental Raman spectrum of PM6.

Figure 2S. Experimental ^{1}H NMR spectrum of PM6.

Figure 3S. Experimental ^{13}C NMR spectrum of PM6.

Figure 4S. UV spectrum of PM6.

Table 1S. Selected geometric parameters Bond length (Å), Bond angle (°) and Dihedral angle (°) of PM6 computed by DFT method (B3LYP/6-311 G (d, p))

Table 2S. Experimental and theoretical wave numbers obtained for (FT-IR and Raman) spectral values of PM6

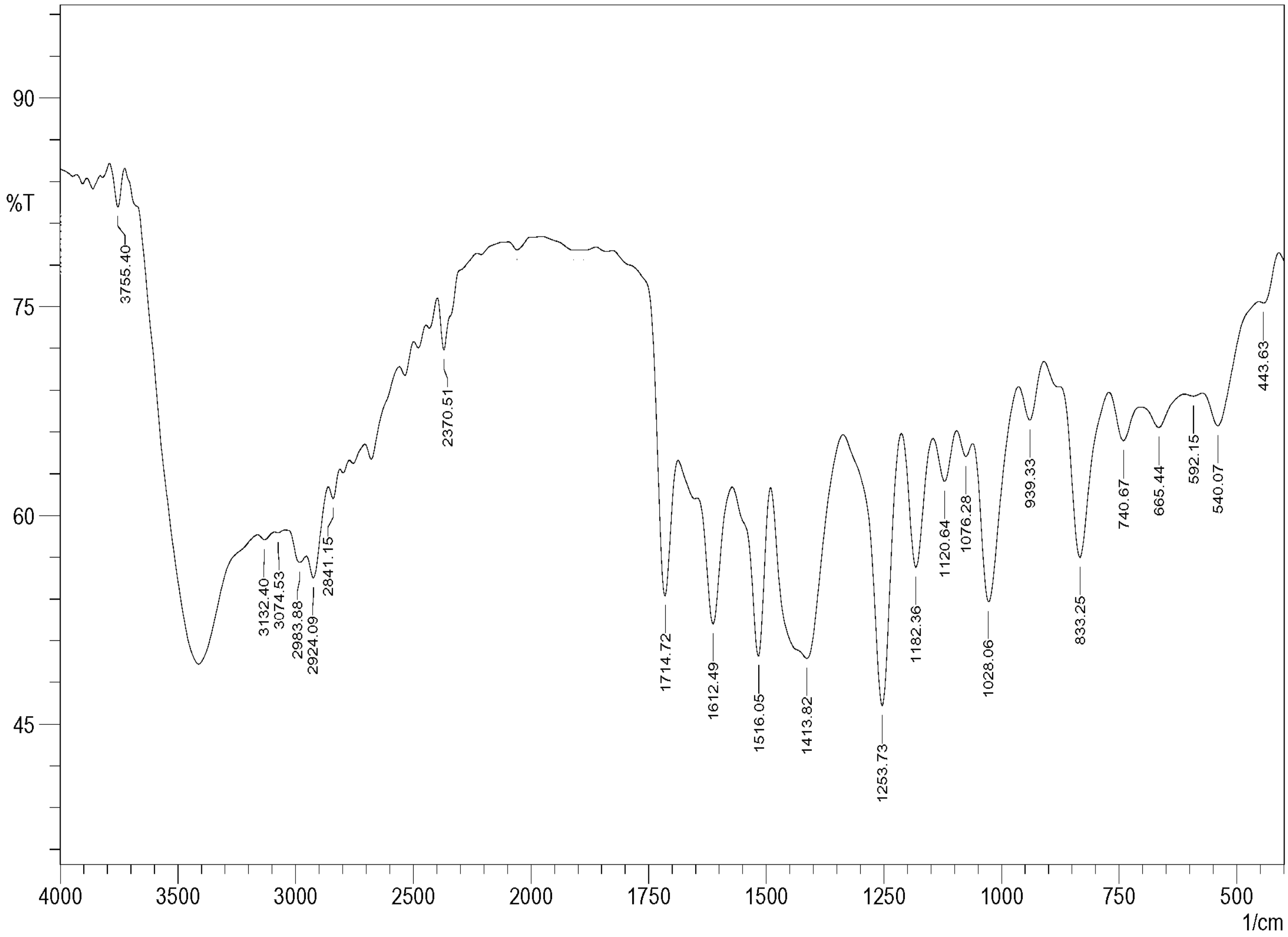

Figure 1S. Experimental IR spectrum of PM6.

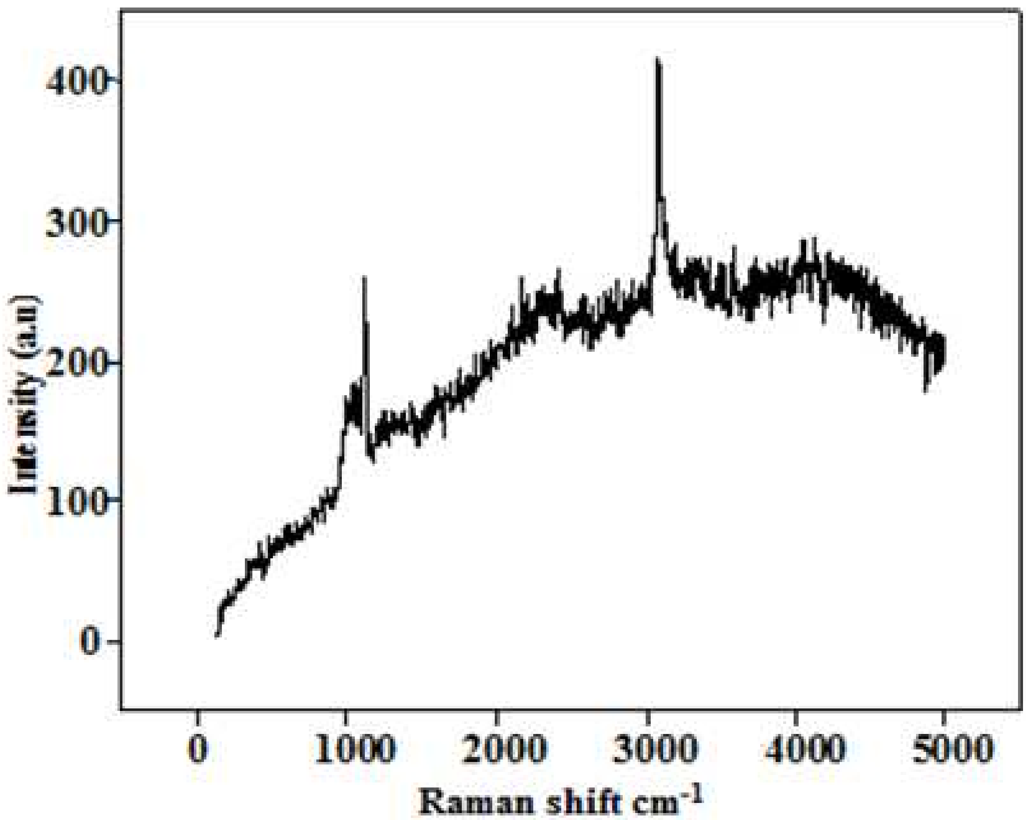

Figure 1S. Experimental Raman spectrum of PM6.

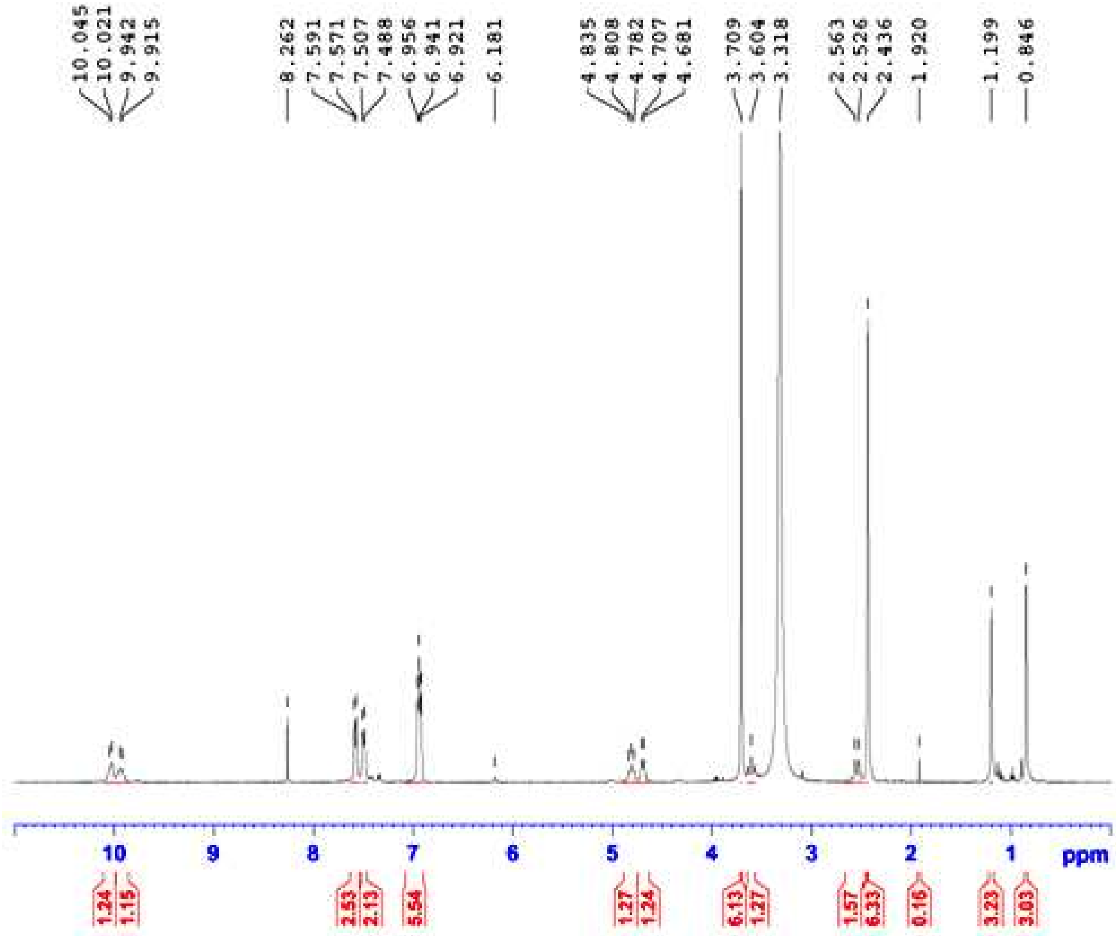

Figure 2S. Experimental ^{1}H NMR spectrum of PM6.

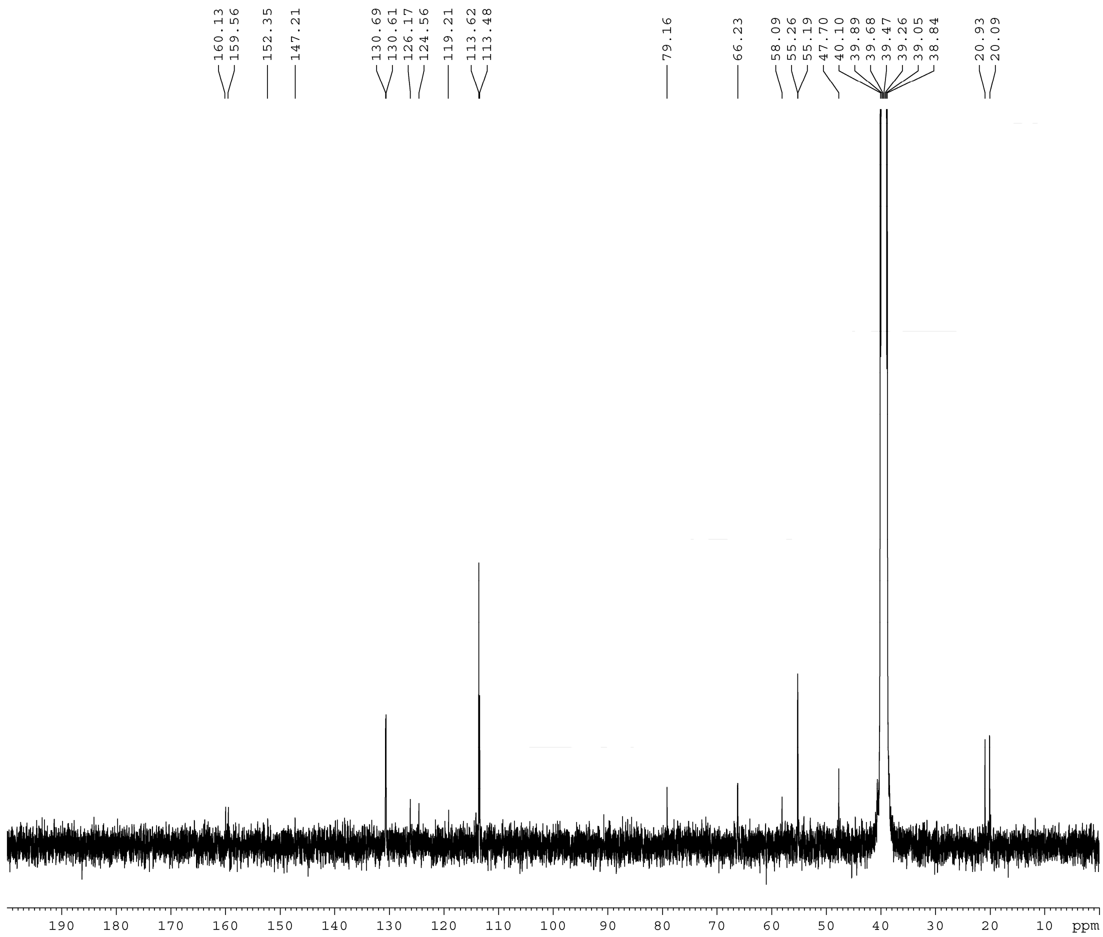

Figure 3S. Experimental ^{13}C NMR spectrum of PM6.

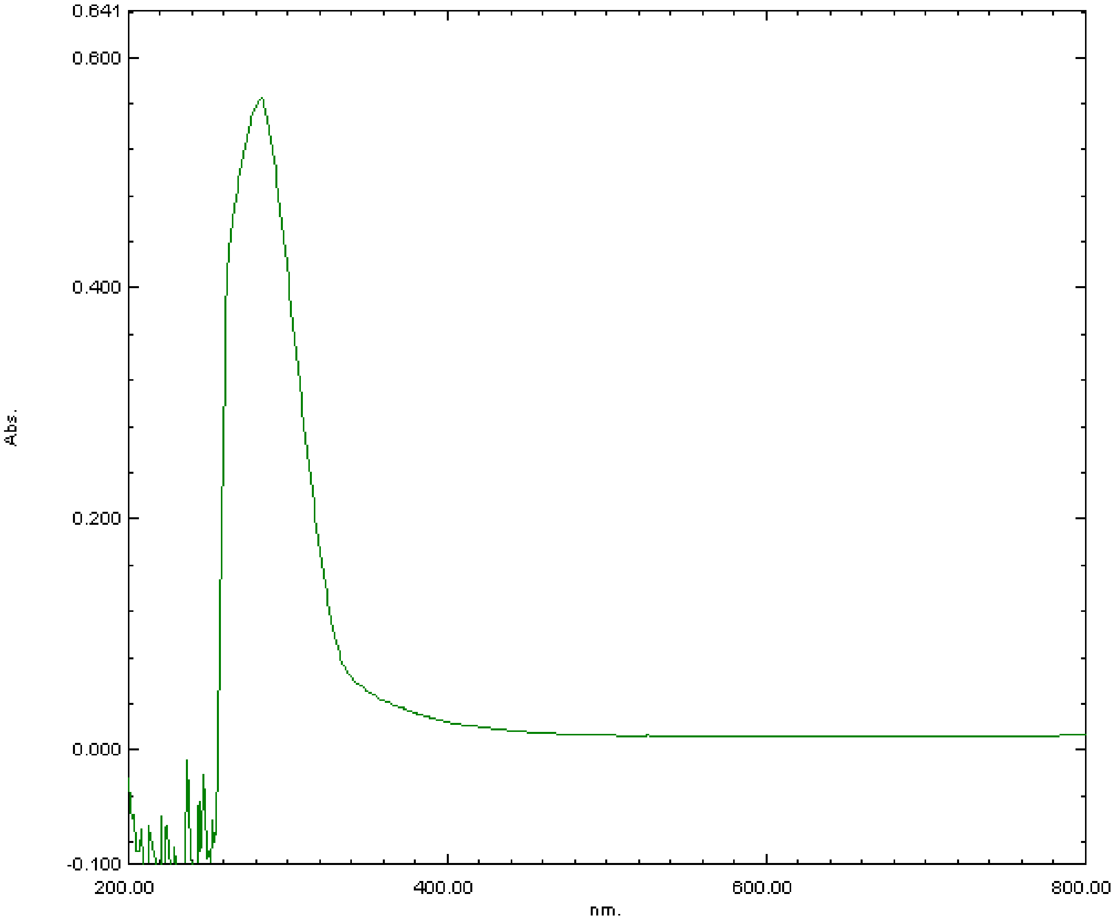

Figure 4S. Experimental UV spectrum of PM6.

Table 1S. Selected geometric parameters Bond Length (A°), Bond Angle (°) and Dihedral angle (°) of PM6 computed by DFT method (B3LYP/6-311 G (d, p)).

Parameters	**Bond Length** (A°)	**Parameters**	**Bond Length** (A°)
C1-N25	1.286	N26-C27	1.378
C1-C16	1.545	C27-C28	1.425
C1-C2	1.511	C27-N32	1.339
C6-C7	1.402	C28-N33	1.414
C6-C11	1.398	C28-N29	1.325
C6-C5	1.521	C31-C30	1.390
C7-C8	1.389	C31-N32	1.334
C11-C10	1.396	C30-N29	1.339
C8-C9	1.401	N33-C37	1.372
C10-C9	1.399	N33-N34	1.365
C9-O12	1.365	C37-C36	1.379
C17-C18	1.406	C37-C39	1.494
C17-C22	1.398	C35-C36	1.420
C17-C15	1.522	C35-N34	1.328
C18-C19	1.388	C35-C38	1.498
C22-C21	1.397	C16-C4	1.546
C19-C20	1.402	C16-C3	1.545
C21-C20	1.398	C16-C15	1.581
C20-O23	1.365	C2-C5	1.543
C13-O12	1.418	N14-C15	1.464
C24-O23	1.418	N14-C5	1.478
N25-N26	1.365		
Parameters	**Bond Angle** (°)	**Parameters**	**Bond Angle** (°)
N25-C1-C16	128.9	C27-C28-N29	120.8
N25-C1-C2	114.1	N33-C28-N29	116.7
C16-C1-C2	116.8	C30-C31-N32	121.7
C7-C6-C11	117.6	C31-C30-N29	120.6
C7-C6-C5	120.5	C28-N33-C37	128.3

C11-C6-C5	121.7	C28-N33-N34	118.9
C6-C7-C8	121.4	C37-N33-N34	112.6
C6-C11-C10	121.7	N33-C37-C36	105.5
C7-C8-C9	120.0	N33-C37-C39	123.5
C11-C10-C9	119.5	C36-C37-C39	130.8
C8-C9-C10	119.4	C36-C35-N34	111.1
C8-C9-O12	115.8	C36-C35-C38	128.5
C10-C9-O12	124.7	N34-C35-C38	120.3
C18-C17-C22	117.4	C37-C36-C35	105.8
C18-C17-C15	122.1	N33-N34-C35	104.8
C22-C17-C15	120.3	C27-N32-C31	117.8
C17-C18-C19	121.3	C28-N29-C30	118.3
C17-C22-C21	122.0	C1-C16-C4	110.8
C18-C19-C20	120.3	C1-C16-C3	110.0
C22-C21-C20	119.4	C1-C16-C15	106.5
C19-C20-C21	119.3	C4-C16-C3	111.1
C19-C20-O23	115.8`	C4-C16-C15	109.3
C21-C20-O23	124.8	C3-C16-C15	108.6
C9-O12-C13	118.1	C1-C2-C5	111.9
C20-O23-C24	118.1	C15-N14-C5	117.3
C1-N25-N26	121.6	C17-C15-C16	115.0
N25-N26-C27	120.6	C17-C15-N14	109.2
N26-C27-C28	125.7	C16-C15-N14	109.0
N26-C27-N32	114.3	C6-C5-C2	111.5
C28-C27-N32	119.9	C6-C5-N14	113.2
C27-C28-N33	122.3	C2-C5-N14	109.6
Parameters	**Dihedral Angle** (°)	**Parameters**	**Dihedral Angle** (°)
C16-C1-N25-N26	-0.6	C1-N25-N26-C27	174.3
C2-C1-N25-N26	178.1	N25-N26-C27-C28	27.7
N25-C1-C16-C4	-63.4	N25-N26-C27-N32	-153.2
N25-C1-C16-C3	59.8	N26-C27-C28-N33	9.5
N25-C1-C16-C15	177.5	N26-C27-C28-N29	-172.9

C2-C1-C16-C4	117.7	N32-C27-C28-N33	-169.4
C2-C1-C16-C3	-118.8	N32-C27-C28-N29	8.0
C2-C1-C16-C15	-1.2	N26-C27-N32-C31	175.8
N25-C1-C2-C5	131.3	C28-C27-N32-C31	-5.0
C16-C1-C2-C5	-49.7	C27-C28-N33-C37	-128.8
C11-C6-C7-C8	0.2	C27-C28-N33-C34	52.8
C5-C6-C7-C8	-178.5	N29-C28-N33-C37	53.5
C7-C6-C11-C10	-0.1	N29-C28-N33-N34	-124.7
C5-C6-C11-C10	178.6	C27-C28-N29-C30	-3.7
C7-C6-C5-C2	102.7	N33-C28-N29-C30	173.9
C7-C6-C5-N14	-132.9	N32-C31-C30-N29	6.2
C11-C6-C5-C2	-76.0	C30-C31-N32-C27	-1.8
C11-C6-C5-N14	48.2	C31-C30-N29-C28	-3.1
C6-C7-C8-C9	-0.2	C28-N33-C37-C36	-178.5
C6-C11-C10-C9	-0.1	C28-N33-C37-C39	2.5
C7-C8-C9-C10	-0.03	N34-N33-C37-C36	-0.1
C7-C8-C9-O12	-179.7	N34-N33-C37-C39	-179.0
C11-C10-C9-C8	0.2	C28-N33-N34-C35	178.5
C11-C10-C9-O12	179.9	C37- N33-N34-C35	-0.003
C8-C9-O12-C13	179.8	N33-C37-C36-C35	0.2
C10-C9-O12-C13	0.1	C39-C37-C36-C35	179.0
C22-C17-C18-C19	-0.8	N34-C35-C36-C37	-0.3
C15-C17-C18-C19	-179.3	C38-C35-C36-C37	179.1
C18-C17-C22-C21	1.2	C36-C35-N34-N33	0.1
C15-C17-C22-C21	179.7	C38-C35-N34-N33	-179.3
C18-C17-C15-C16	-87.5	C1-C16-C15-C17	177.5
C18-C17-C15-N14	35.3	C1-C16-C15-N14	54.3
C22-C17-C15-C16	93.9	C4-C16-C15-C17	57.6
C22-C17-C15-N14	-143.0	C4-C16-C15-N14	-65.4
C17-C18-C19-C20	-0.01	C3-C16-C15-C17	-63.9
C17-C22-C21-C20	-0.6	C3-C16-C15-N14	172.9
C18-C19-C20-C21	0.5	C1-C2-C5-C6	171.9

C18-C19-C20-O23	-179.8	C1-C2-C5-N14	45.6
C22-C21-C20-C19	-0.2	C5-N14-C15-C17	171.8
C22-C21-C20-O23	-179.7	C5-N14-C15-C16	-61.6
C19-C20-O23-C24	-179.9	C15-N14-C5-C6	-116.1
C21-C20-O23-C24	-0.4	C15-N14-C5-C2	9.1

Table 2S. Experimental and theoretical wave numbers obtained for (FT-IR) spectral values of PM6.

Mode Nos	IR	Raman	Unscaled	Scaled	I_{IR}	I_{Raman}	Vibration Assignments (TED≥100)
1			11	10	3.38	4.9	ƮN25 N26 C27 C28 (35)+ƮN26 N25 C1 C2 (13)+ ƮC2 C15 C5 N14 (10)
2			18	17	1.97	5.41	ƮC1 N25 N26 C27 (37)+ƮC5 N14 C2 C1 (15)+ ΓN25 C1 C2 C16 (10)
3			20	19	1.86	6.5	ƮC21 C16 N14 C5 (14)
4			24	23	4.48	7.03	βN25 N26 C27 (14)+ ƮN14 C5 C6 C11 (23)
5			26	25	1.65	8.3	ƮN14 C5 C6 C11 (37)+ ΓC15 C17 C22 C18 (10)
6			36	34	6.33	10.19	ƮN34 N33 C28 N29 (27)+ΓC28 C27 N34 N33 (11)
7			40	38	1.32	8.51	ƮN34 N33 C28 N29 (11)
8			46	44	1.96	4.43	ƮN34 N33 C28 N29 (17)+ƮC2 C15 C5 N14 (14)+ ΓC28 C27 N34 N33 (13)
9			58	55	6.72	7.38	ƮN14 C15 C17 C22 (52)
10			68	65	3.22	5.85	ƮN34 N33 C28 N29 (11)
11			80	77	4.18	6.07	ƮC13 O12 C9 C8 (10)+ΓN33 C28 N29 C27 (11)+ ΓC28 C27 N34 N33 (19)
12			84	81	7.31	6.59	βC28 N33 N34 (12)+ ƮC31 N32 C30 N29 (13)+ ΓN33 C28 N29 C27 (11)
13			93	89	8.24	6.18	ƮC13 O12 C9 C8 (26)+ ƮC24 O23 C20 C19 (23)
14			107	103	8.84	2.09	ƮC13 O12 C9 C8 (21)+ ƮC24 O23 C20 C19 (15)
15			114	110	3.43	5.33	ƮH38 C38 C35 C36 (12)+ƮH38 C38 C35 C36 (12)

16		116	111	3.29	4.89	βC22 C17 C15 (11)
17		128	123	2.37	2.59	ƮH39 C39 C37 N33 (13)+ βC11 C6 C5 (10)
18		161	155	7.31	2.23	ƮC9 C8 C10 C11 (13)+ ƮC13 O12 C9 C8 (11)
19		178	171	4.27	3.03	ƮH4 C4 C16 C3 (17)+ƮH4 C4 C16 C3 (13)+ ƮH3 C3 C16 C4 (10)
20		180	173	11.49	8.24	ƮC31 N32 C30 N29 (16)+ГC39 N33 C36 C37 (10)
21		192	185	1.77	6.07	ƮH39 C39 C37 N33 (13)+ƮC36 C37 C35 N34 (12)+ГC38 C36 N34 C35 (14)+ ГC39 N33 C36 C37 (19)
22		203	195	8.56	5.01	ƮH3 C3 C16 C4 (10)+ βC4 C16 C1 (12)
23		224	216	2.18	2.66	βC39 C37 C36 (10)
24	217	226	218	9.94	5.27	βO23 C20 C21 (22)+ βC24 O23 C20 (18)
25		236	227	6.63	1.36	βC39 C37 C36 (10)
26		250	241.25	7.64	4.94	ƮH13 C13 O12 C9 (12)+ƮH13 C13 O12 C9 (10)+βC39 C37 C36 (14)+ βC38 C35 N34 (11)
27		258	248	1.86	5.42	ƮH24 C24 O23 C20 (24)+ƮH24 C24 O23 C20 (11)+ ƮH24 C24 O23 C20 (15)
28		268	258	7.03	6.7	βC3 C16 C1 (21)
29		279	269	7.44	3.28	βO12 C9 C10 (13)+ βC13 O12 C9 (18)
30		299	288	14.61	6.77	βC38 C35 N34 (10)
31		307	296	7.38	3.31	βC16 C15 N14 (13)+ ГC4 C15 C1 C16 (22)
32	299	311	300	5.96	7.11	ГC38 C36 N34 C35 (13)+ГC39 N33 C36 C37 (10)

33			321	309	5.13	10.67	βC38 C35 N34 (12)
34			343	331	12.33	3.56	βC22 C17 C15 (19)+ βC24 O23 C20 (12)
35			369	356	4.96	11.58	ƮN26 N25 C1 C2 (32)+ ΓC4 C15 C1 C16 (13)
36			373	359	10.29	7.63	ΓC3 C4 C1 C16 (17)
37			395	381	9.53	8.99	ƮC10 C9 C11 C6 (10)+ƮN26 N25 C1 C2 (13)
38		394	411	396	5.52	3.85	ΓC3 C4 C1 C16 (18)
39			424	409	4.89	1.3	ƮH7 C7 C8 C9 (12)+ƮH11 C11 C10 C9 (14)+ƮC9 C8 C10 C11 (27)+ƮC8 C7 C9 C10 (37)
40			431	415	3.02	1.52	ƮC21 C20 C22 C17 (12)+ƮC20 C19 C21 C22 (20)+ ƮC19 C18 C20 C21 (28)
41			437	421	12.7	4.16	ƮC21 C20 C22 C17 (15)
42	443	441	462	445	7.39	5.84	βC10 C9 C8 (10)+ βC13 O12 C9 (14)
43			468	451	6.99	5.03	βO23 C20 C21 (11)+ βC24 O23 C20 (23)
44			506	488	14.05	13.07	ƮH26 N26 N25 C1 (31)
45		498	518	499	18.97	11.92	ƮH26 N26 N25 C1 (11)+βC5 N14 C15 (10)
46			546	526	29.31	5.61	ΓO23 C19 C21 C20 (10)
47			556	536	26.46	19.05	ƮH26 N26 N25 C1 (16)+ΓN26 C28 N32 C27 (19)
48			573	552	20.48	6.03	ΓC6 C2 N14 C5 (10)
49			589	568	8.46	7.75	νC39 C37 (13)+βC35 C36 C37 (12)+ƮC30 C27 C31 N32 (11)+ƮC30 C31 N29 C28 (11)

50			600	579	5.51	9.25	νC38 C35 (14)+βC35 C36 C37 (18)+ ƮC30 C27 C31 N32 (12)
51			637	614	9.31	8.79	βC31 C30 N29 (12)+ƮC36 N34 C37 N33 (14)
52			649	626	9.55	9.8	νC20 C19 (10)+βC22 C21 C20 (18)+ βC20 C19 C18 (32)
53			654	631	11.43	5.85	ƮH39 C39 C37 N33 (10)+ƮC36 N34 C37 N33 (36)
54			655	632	7.22	7.84	βC9 C8 C7 (25)
55			672	648	16.62	6.84	ΓN25 C1 C2 C16 (12)
56			679	655	10.47	6.98	ƮH38 C38 C35 C36 (11)+ƮC36 C37 C35 N34 (50)+ ΓC38 C36 N34 C35 (13)
57	665	665	689	664	20.98	7.06	νC3 C16 (10)
58			713	688	36.38	7.3	βC30 C31 N32 (14)+ ƮC10 C9 C11 C6 (12)
59			729	703	11.2	4.37	ƮC21 C20 C22 C17 (17)
60			745	718.	12.04	4.91	ƮC10 C9 C11 C6 (24)
61		720	750	723	11.89	6.36	ƮC21 C20 C22 C17 (10)
62	740	743	779	751	18.08	4.89	νN33 C37 (10)+νC39 C37 (11)+νC38 C35 (10)
63			791	763	9	10.07	νC21 C20 (16)+νC20 C19 (10)+νO23 C20 (15)+ ΓC17 C16 N14 C15 (10)
64			795	767	21.16	5.79	ƮH36 C36 C35 C38 (74)
65			802	773	12.35	12.21	ƮH36 C36 C35 C38 (14)+ƮC30 C27 C31 N32 (13) +ƮC30 C31 N29 C28 (12)+ ΓN26 C28 N32 C27 (14)+ΓN33 C28 N29 C27 (11)
66			811	782	7.6	17.5	νC10 C9 (17)+νC9 C8 (12)+ νO12 C9 (28)

67			826	797	14.78	6.63	ƮH11 C11 C10 (25)+ ƮH8 C8 C9 C10 (11)+ ƮH10 C10 C9 C8 (46)
68			829	799	19.53	10.64	ƮH22 C22 C21 C20 (22)+ƮH21 C21 C20 C19 (47)
69			839	809	18.47	17.24	ƮH19 C19 C20 C21 (10)
70		816	848	818	30.27	9.63	ƮH7 C7 C8 C9 (27)+ƮH8 C8 C9 C10 (30)+ ΓO12 C8 C10 C9 (15)
71			858	827	27.18	13.33	ƮH18 C18 C19 C20 (11)+ƮH19 C19 C20 C21 (19)+ ƮH30 C30 N29 C28 (11)
72			862	831	22.48	5.22	ƮH19 C19 C20 C21 (12)+ƮH30 C30 N29 C28 (29)+ ƮH31 C31 N32 C27 (12)
73	833	834	865	834	13.78	14.55	ƮH30 C30 N29 C28 (23)
74			920	887	21.68	12.4	βC31 N32 C27 (15)+ βC31 C30 N29 (22)
75			935	902	9.14	10.56	νC4 C16 (11)+νC3 C16 (15)+νC15 C16 (11)
76			936	903	10.91	12.66	ƮH11 C11 C10 C9 (16)+ ƮH10 C10 C9 C8 (13)+ νC2 C5 (21)
77		910	948	914	9.03	9.89	ƮH11 C11 C10 C9 (21)+ƮH10 C10 C9 C8 (10)+ νC4 C16 (11)
78			951	917	11.86	8.63	ƮH22 C22 C21 C20 (13)+ νC3 C16 (10)
79			955	921	4.09	4.71	ƮH22 C22 C21 C20 (36)+ƮH21 C21 C20 C19 (15)
80			959	925	5.92	5.32	ƮH30 C30 N29 C28 (26)+ƮH31 C31 N32 C27 (62)
81			964	930	3.43	3.48	ƮH7 C7 C8 C9 (48)+ƮH8 C8 C9 C10 (37)
82	939	946	984	949	3.97	2.12	ƮH18 C18 C19 C20 (56)+ƮH19 C19 C20 C21 (28)
83			990	955	23.43	9.82	βH36 C36 C35 (12)+ƮH38 C38 C35 C36 (10)+ νC35 C36 (19)

84			1002	966	7.94	6.46	ƮH39 C39 C37 N33 (18)+ ƮH39 C39 C37 N33 (15)+ƮH38 C38 C35 C36 (10)+ ƮH38 C38 C35 C36 (10)
85			1019	983	14.78	6.7	βH2 C2 C1 (13)
86			1027	991	9.47	2.38	βH8 C8 C9 (10)+βC11 C10 C9 (37)+ βC10 C9 C8 (12)+ βC9 C8 C7 (26)
87			1029	992	3.41	2.28	βH19 C19 C20 (10)+ νN14 C15 (10)+ βC22 C21 C20 (31)+ βC21 C20 C19 (12)+ βC20 C19 C18 (25)
88			1041	1004	11.22	13.64	βC35 C36 C37 (26)
89			1043	1006	8.94	6.58	ƮH4 C4 C16 C3 (18) + ƮH3 C3 C16 C4 (17)
90			1054	1017	34.05	18.99	βC37 N33 N34 (20)
91		1022	1065	1027	6.79	4.78	βH38a C38 H38c (13)+ βH38c C38 H38b (14)+ ƮH38 C38 C35 C36 (19)+ ƮH38 C38 C35 C36 (23)+ ƮH38 C38 C35 C36 (23)
92	1028	1026	1070	1032	11.62	3.26	βH39a C39 H39c (13)+ βH39b C39 H39a (11)+ ƮH39 C39 C37 N33 (26)+ ƮH39 C39 C37 N33(18)+ ƮH39 C39 C37 N33 (21)
93			1076	1038	68.12	8.23	νO12 C13 (39)+ νO23 C24 (34)
94			1077	1039	76.03	11.63	νO12 C13 (33)+ νO23 C24 (38)
95			1098	1059	40.5	14.02	νN14 C15 (20)
96			1103	1064	34.29	29.45	νC30 C31 (25)+ νN25 N26 (10)
97	1076	1079	1129	1089	40.72	15.51	νN25 N26 (13)+ νN14 C15 (10)+ νC2 C5 (10)
98			1136	1096	26.21	3.8	βH8 C8 C9 (14)
99			1142	1102	20.72	4.82	βH18 C18 C19 (15)+ βH19 C19 C20 (15)

100			1148	1107	49.31	10.74	νN25 N26 (26)
101	1120	1123	1165	1124	30.2	10.27	νN33 N34 (26) + νN14 C5 (10)+ νC4 C16 (11)
102			1170	1129	29.93	8.34	βH36 C36 C35 (40)+ νN33 N34 (13)+ νC39 C37 (13)
103			1173	1131	49.34	3.91	ƮH4 C4 C16 C3 (13)+ νC1 C2(14)
104			1178	1136	4.33	7.93	βH24a C24 H24c (14)+ βH24b C24 H24a (14)+ ƮH24 C24 O23 C20 (38)+ ƮH24 C24 O23 C20 (16)+ ƮH24 C24 O23 C20 (17)+ ƮH24 C24 O23 C20 (17)
105			1179	1137	3.85	7.8	βH13a C13 H13c (13)+ βH13 bC13 H13a (14)+ ƮH13 C13 O12 C9 (38)+ ƮH13 C13 O12 C9 (17)+ ƮH13 C13 O12 C9 (17)
106			1199	1157	26.58	9.2	νN33 N34 (18)
107			1200	1158	17.31	13.6	νN33 N34 (20)
108			1203	1160	41.4	14.03	βH22 C22 C21 (10)
109			1211	1168	13.46	7.82	βH13C13H13 (16)+ ƮH13 C13 O12 C9 (27)+ ƮH13 C13 O12 C9 (29)
110			1212	1169	17.15	11.87	βH24c C24 H24b (15)+ ƮH24 C24 O23 C20 (26)+ ƮH24 C24 O23 C20 (26)
111	1182	1184	1228	1185	13.64	19.59	νC17 C15 (20)
112			1246	1202	19.41	20.67	ƮH2 C2 C1 C16 (20)+ νC6 C5 (11)
113			1270	1225	27.05	15.44	νC1 C2 (16)
114		1227	1277	1232	29.74	18.16	νN29 C28 (22)+ νN32 C27 (23)+ νC27 C28 (13)
115			1294	1248	96.24	11.06	νO12 C9 (28)+ νO23 C20 (10)

116			1295	1249	89.1	14.52	νC22 C21 (11)+ νO23 C20 (30)
117	1253	1253	1303	1257	55.28	17.77	βH2 C2 C1 (13)+ βH5 C5 C6 (14)+ ƮH2 C2 C1 C16 (10)
118			1307	1261	20.24	19.77	βH26 N26 N25 (11)+ νN32 C31 (17)+ νN29 C30 (19)+ νN26 C27 (10)
119			1323	1276	14.79	11.38	βH18 C18 C19(17)
120			1331	1284	15.09	16.88	βH7 C7 C8 (11)+ βH11 C11 C10 (10)
121			1332	1285	6.42	17.11	νN32 C31(10)+ νN33 C37(12)
122			1344	1296	38.64	11.51	βH22 C22 C21 (10)
123			1346	1298	37.86	11.67	ƮH5 C5 C6 C7 (11)+ νC10 C9 (13)
124			1353	1305	10.63	15.37	ƮH15 C15 C17 C18 (31)+ ƮH5 C5 C6 C7(13)
125			1374	1325	13.12	33.19	ƮH2 C2 C1 C16 (11)+ ƮH15 C15 C17 C18 (25)+ ƮH5 C5 C6 C7 (30)
126			1396	1347	29.41	10.32	βH15 C15 C17 (14)+ βH5 C5 C6 (30)
127			1404	1354	34.88	17.55	βH38a C38 H38c (10)+ βH38b C38 H38a (11)+ βH38c C38 H38b (10)+ νC35 C36(12)
128			1405	1355	21.91	11.38	βH15 C15 C17 (29)+ βH5 C5 C6 (13)
129			1417	1367	16.03	6.63	βH4 C4 H4 (20)+ βH4 C4 H4 (20)+ βH3 C3 H3 (17)+ βH3 C3 H3 (11)+ βH3 C3 H3 (11)
130			1424	1374	36.61	17.83	βH38a C38 H38c (13)+ βH38c C38 H38b (13)+ βC37 N33 N34 (10)
131			1425	1375	8.4	11.57	βH39a C39 H39c (26)+ βH39b C39 H39a (36)+

							βH39c C39 H39b (29)
132			1435	1384	27.85	14.18	βH4a C4 H4c (11)+ βH4b C4 H4a (15)+ βH3a C3 H3c (15)+ βH3b C3 H3a (17)+ βH3c C3 H3b (12)
133			1456	1405	40.21	5.37	βH26 N26 N25 (20)+ βH31 C31 N32 (32)
134			1461	1409	25.9	10.88	βH14 N14 C5 (12)+ νC19 C18 (11)+ νC22 C21 (10)
135			1462	1410	35.91	8.72	νC35 C36 (21)
136	1413	1407	1466	1414	7.23	4.61	νC8 C7 (12)+ νC11 C10 (11)+ βH24b C24 H24a (33)
137			1480	1428	47.32	19.14	βH14 N14 C5 (46)
138			1483	1431	57.28	15.85	νC38 C35 (12)
139			1488	1435	18.82	11.65	βH24a C24 H24c (28)+ βH24b C24 H24a (33)+ βH24c C24 H24b (18)
140			1489	1436	20.3	9.86	βH13a C13 H13c (32)+ βH13b C13 H13a (30)+ βH13c C13 H13b (18)
141			1491	1438	11.61	15.71	βH39a C39 H39c (40)+ βH39b C39 H39a (35)+ τH39 C39 C37 N33 (17)
142			1495	1442	9.98	11.38	βH4b C4 H4a (16)+ βH4c C4 H4b (21)+ βH2b C2 H2a (28)
143			1496	1443	11.3	12.3	βH4b C4 H4a (12)+ βH4c C4 H4b (12)+ βH2b C2 H2a (45)

144		1498	1445	14.23	15.53	βH38a C38 H38c (35)+ βH38c C38 H38b (40)+ ƮH38 C38 C35 C36 (15)
145		1503	1450	75.54	23.96	βH24a C24 H24c (37)
146		1504	1451	68.92	48.21	βH13b C13 H13a (37)+βH38b C38 H38a (33)+ ƮH24 C24 O23 C20 (16)
147		1505	1452	100	74.45	βH13b C13 H13a (38)+ βH24b C24 H24a (39)+ ƮH13 C13 O12 C9(16)
148		1510	1457	8.79	11.03	βH3a C3 H3c (34)+ βH3b C3 H3a (18)
149		1513	1460	15.96	15.4	βH4c C4 H4b (16)+ βH3b C3 H3a (27)+ βH3c C3 H3b (27)+ ƮH3 C3 C16 C4 (10)
150		1518	1464	20.46	9.55	βH39a C39 H39c (11)+ βH39c C39 H39b (36)
151		1519	1465	73.82	23.97	βH13c C13 H13b (41)+ βH24c C24 H24b (16)
152		1521	1467	23.15	5.32	βH13c C13 H13b (17)+ βH24c C24 H24b (41)
153		1522	1468	31.65	10.09	βH4a C4 H4c (24)
154		1533	1479	40.52	17.97	βH38b C38 H38a (16)+ νN34 C35 (13)+ νN33 C37 (10)
155		1550	1495	87.43	16.34	βH26 N26 N25 (23)+ νN26 C27 (14)
156		1557	1502	62.19	8.75	βH18 C18 C19 (11)+ νC20 C19 (11)+ νC18 C17 (11)
157		1559	1504	56.68	11.94	βH7 C7 C8 (11)+ βH10 C10 C11 (10)+ νC7 C6 (10)+ νC9 C8 (10)
158		1597	1541	77.74	53.5	νN29 C28 (21)+ νN32 C27 (23)+ νN29 C30 (17)
159		1616	1559	49.69	32.2	νC36 C37 (21)+ νN34 C35 (12)+ νC30 C31 (10)
160	1563	1625	1568	40.87	40.28	νC36 C37 (19)+ νC30 C31 (12)+ νC27 C28 (10)
161		1628	1571	17.3	12.04	νC17 C22 (17)+νC21 C20 (25)+νC20 C19 (13)+ νC18 C17 (18)
162		1631	1573	19.34	10.34	νC6 C11 (18)+νC7 C6 (18)+νC10 C9 (23)+ νC9

							C8 (15)
163			1670	1611	46.59	39.2	νC19 C18 (16)+ νC17 C22 (11)+ νC22 C21 (13)
164	1612	1612	1671	1612	41.3	43.59	νN25 C1 (79)
165			1698	1638	19.61	100	νC8 C7 (17)+νC6 C11 (10)+ νC11 C10 (14)
166			2927	2824	31.38	16.53	νC15 H15 (99)
167			2991	2886	29.67	28.26	νC5 H5 (95)
168			3014	2908	67.23	78.46	νC13 H13c (45)+ νC24 H24c (45)
169			3015	2909	82.91	84.79	νC13 H13b (45)+ νC24 H24b (44)
170		2913	3030	2923	25.17	28.81	νC2 H2 (91)
171	2924	2923	3041	2934	32.69	48.91	νC38 H38a (41)+ νC38 H38b (43)+ νC38 H 38c (16)
172			3049	2942	23.26	42.43	νC39 H39a (19)+νC39 H39b (22)+νC39 H39c (59)
173			3054	2947	22.84	31.65	νC3 H3a (30)+ νC3 H3b (14)+νC3 H3c (54)
174		2944	3064	2956	21.44	47.53	νC4 H4a (27)+ νC4 H4b (37)+νC4 H4c (35)
175			3075	2967	56.23	43.64	νC13 H13c (50)+ νC24 H24c (49)
176			3076	2968	68.32	52.25	νC13 H13b (49)+ νC24 H24b (50)
177			3094	2985	26.06	37.13	νC38 H38a (51)+ νC38 H38b (49)
178	2983	2983	3112	3003	18.96	28.86	νC39 H39a (12)+ νC39 H39b (49)+ νC39 H39c (39)
179			3122	3012	22.87	30.72	νC3 H3a (48)+ νC3 H3c (43)

180			3128	3018	34.94	26.08	νC4 H4b (58)+ νC4 H4c (34)
181			3135	3025	15.57	25.98	νC2 H2 (95)
182			3141	3031	16.31	26.49	νC38 H38c (84)
183			3143	3033	19.72	28.55	νC39 H39a (69)+ νC39 H39b (28)
184			3146	3035	18.71	25.97	νC4 H4 (63)+ νC4 H4 (27)
185			3148	3037	28.36	29.5	νC3 H3 (19)+ νC3 H3 (72)
186			3149	3038	43.87	82.09	νC13 H13 (54)+ νC24 H24b (37)
187			3150	3039	56.02	95.39	νC13 H13 (37)+ νC24 H24a (54)
188	3059	3053	3175	3063	18.6	42.99	νC31 H31 (39) + νC16 H16 (59)
189			3176	3064	21.64	26.36	νC11 H11 (88)+ νC30 H30 (21)
190			3177	3065	17.59	26.68	νC7 H7 (87)
191			3179	3067	19.19	22.27	νC22 H22 (96)
192	3074	3074	3198	3086	36.86	73.12	νC30 H30 (79)+ νC31 H31 (21)
193			3203	3090	12.92	32.99	νC18 H18 (29)+νC19 H19 (70)
194		3088	3211	3098	15.4	46.57	νC8 H8 (94)
195			3219	3106	13.06	33.16	νC18 H18 (68)+νC19 H19 (29)
196		3098	3222	3109	35.49	77.41	νC21 H21 (93)
197	3132	3133	3259	3144	10.55	36.64	νC36 H36 (99)

198			3561	3436	30.94	66.12	νN26 H26 (99)
199	3412	3425	3563	3438	6.18	35.47	νN14 H14 (99)

ν - stretching, β - inplane bending, τ - torsional vibrations, Γ - out of plane bending

Highlights:

1. PM6 was synthesized and characterized by IR, ^{1}H, ^{13}C NMR, UV and Raman spectroscopy.
2. Optimized geometry, HOMO-LUMO, MEP, Polarizability, NBO and Docking were discussed.
3. ^{1}H and ^{13}C NMR chemical shifts have been compared with experimental values.
4. Theoretical IR frequencies are analysed by TED% using VEDA 4 program.
5. Computational technique were carried out by B3LYP/6-311G (d, p) basis set.